



Wireless Power Transmission for Biomedical Applications

An Honors Thesis for the
Department of Electrical
Engineering

Cynthia M. Wisnieff

**Tufts University
School of Engineering 2009**

Cynthia M. Wisnieff

Dr Sameer Sonkusale
Department of Electrical Engineering
Tufts University

Dr David Kaplan
Department of Biomedical Engineering
Tufts University

Dr. Ronald Lasser
Department of Electrical Engineering
Tufts University

Table of Contents

Abstract.....	1
Introduction.....	2
Background.....	4
Electromagnetism	4
Transformers.....	6
Class E Power Amplifier	9
Rectifier Circuits.....	11
Radio Frequency Tissue interactions.....	12
Silk Polymer Overview.....	13
Methods.....	14
System Overview	14
Coil Design	15
Coil Simulations.....	17
Final Coil Design	22
Radio Frequency Safety Calculations.....	25
Class E Power amplifier design	27
Receiver Tuning Calculations.....	28
Summary of System Parameters	29
Experimental Verification of Coil Behavior.....	30
Novel Experiments.....	31
Results.....	32
Experimental Coil Measurements.....	32
Silk Experiment Results.....	39
Analysis.....	41
Coil Experimental Analysis	41
Silk Experimental Analysis.....	43
Discussion.....	44
Coil Experimental Discussion.....	45
Silk Experimental Discussion	47
Future Work	50
Appendix.....	53
VBA code for individual coils	53
VBA code for simulating coil pairs	59
References.....	73

Table of Figures

Figure 1: Transformer circuit diagram.....	6
Figure 2: Simple class E power amplifier schematic.....	9
Figure 3: Design equations for a class E power amplifier developed by Sokal.	10
Figure 4: Diagram of a half wave rectifier.....	11
Figure 5: Picture of petri dish with electrode setup showing gel formation.....	14
Figure 6: System diagram depicting the full system.....	14
Figure 7: Graph depicting effect of variation in transmitter coil parameters.	18

Figure 8: Depiction of an alternative view of varying transmitter coil dimensions.	19
Figure 9: A graph depicting variations in the coupling coefficient due to the number of turns of the transmitter.	20
Figure 10: Receiver coil parameters on coupling coefficient	21
Figure 11: Effects of rotating coils in space and the effect on coupling.....	23
Figure 12: Variation in coupling over xy plane.	24
Figure 13: Graph showing the simulated variation in coupling coefficient along the z axis	25
Figure 14: FastHenry depiction of coils.....	25
Figure 15: Coupling coefficient between the final coils along a line outward from the center of the transmitter with 1mm separation between the coils.....	26
Figure 16: Diagram of Thevenin equivalent circuit with load.....	34
Figure 17: Measured and Simulated values of coupling coefficient as a function of separation close to coils.	36
Figure 18: Log-log plot of the effect of separation between coils on the coupling coefficient for the measured range of 0-19 cm.	37
Figure 19: Plot of all measured and simulated data for coupling as a function of distance.	38
Figure 20: Comparison of coupling when coils are rotated with respect to each other....	39
Figure 21: Image showing degree of gel formation in the silk after a week.	39
Figure 22: Picture showing differential build-up of silk.....	40
Figure 23: Diagram of PCB used for the final coil designs.....	71
Figure 24: Screen view of coil pair simulator.....	72
Figure 25: Screen view of individual coil simulator.....	73

List of Tables

Table 1: Dielectric Parameters for muscle tissue at various frequencies (9).....	12
Table 2: Final coil design parameters	22
Table 3: FastHenry estimates of inductance, series resistance and Q.....	22
Table 4: Table showing system component parameters	29
Table 5: Experimentally determined values of inductors	32
Table 6: Table comparing simulated and experimental values of designed coils.....	33
Table 7: Coil parameters and effects on transmission between coils	45
Table 8: Experimental parameters and predicted output relationship for silk experiments	47

Abstract

This investigation explores a method of designing planar spiral coils for the purpose of transmitting power wirelessly for biomedical applications. The designed coils were integrated into a system that will generate and receive the wireless signal. The primary focus of this investigation will be to explore the affects of changing the geometry of the coils on the power transmission characteristics of the system. This will be investigated through both simulation and experimental verification. The second task of this investigation will be to use the system in a novel experiment to explore the effects of electric fields on an aqueous silk solution.

The system consists of two main components a transmitter and a receiver. The transmitter consists of a class E power amplifier where the transmitter coil is the inductor of the resonant circuit. The receiver circuit consists of the receiver coil and a capacitor that forms a resonant tank and a half wave rectifier to produce the output signal from the transmitter. The coils will be designed using an iterative method that will rely on a software tool called FastHenry to model inductors of specific geometries. After completing the design and construction of the system it will be used in two novel experiments. The experiments aim to investigate novel methods of inducing a silk solution to form a gel.

Introduction

Biomedical devices, such as biomedical implants, that require energy over an extended lifespan and the ability to process information remotely have previously relied on batteries as sources of power. These systems are limited by the life span and maintainability of these batteries. Wired external sources must use wires that pass through the skin. This passage opens the site of the implant to the environment and possible infection as the skin will not be able to protect the area where the wires must pass (1). Implants with a battery source have a limited lifespan even if the battery itself is wirelessly rechargeable as it also has a limited number of useful charge and discharge cycles (1). This limited lifespan prevents extended use of the implant and requires further maintenance than if both power and data could be transmitted wirelessly.

Wireless power delivery solves the problem of crossing the skin to deliver power and the requirement of having a limited implanted source of power. There are currently several proposed methods of obtaining power wirelessly from the environment of the implant; which include thermoelectric, light, vibration and heel strike (2). An inductive link however has the added advantage of not only being able to provide power to the implant, but it is also able to transmit data wirelessly. Wireless transmission of power and data removes the implanted power source and the need to perform certain computations on data gathered by the device that can be sent outside the body to an external processor which can then send the appropriate information back to the implant to take action. More efficient links in biomedical implants will improve the practicality of systems that are currently in use such as cochlear implants and systems that are being developed such as retinal implants and deep brain implants (2). Therefore the focus of this senior design

project is to design coils and develop a system to deliver power to a biomedical device wirelessly.

Optimizing the geometry of the coils and the materials used to construct them will help lead to an increase in the coupling coefficient of the coils and a decrease the volume associated with the implanted coil. Increasing the coupling coefficient of the coils is directly related to the power transfer efficiency, where increased coupling will allow for greater power transfer. With increased coupling strength the receiver can operate over a greater range, which allows for the location of the implant to be more flexible; such as at greater depths. Optimizing the geometry of the coils to minimize its volume decreases the volume necessary for a biomedical implant, which makes the implant itself less intrusive. This can be accomplished using spiral coils that spiral inwards towards the center of the coil as apposed to columnar coils, for example. Since planar spiral coils offer an advantage to implantable biomedical applications the coils designed in this investigation will aim to optimize coupling in environments that include this possible application though there is no specific task currently designated for these coils.

Background

Electromagnetism

Inductive links rely on Faraday's law of induction to remotely induce currents in a loop of wire due to the presence of an external electromagnetic field. The presence of a changing electric field will produce a change in magnetic flux through a closed surface bounded by a conductor. This change in magnetic flux produces a current in the loop of conductor. An inductor is a passive circuit element that can create and react to electromagnetic fields. Properties of inductors are highly dependent on the specific geometry of the conductor and material of the conductor. For example a single loop of wire, R_1 is the radius of the loop and r is the radius of the wire has self inductance of:

Equation 1

$$L(R_1, r) = \mu_0 R_1 \left(\ln \left(\frac{8R_1}{r} \right) - 2 \right)$$

Expanding this formula for a stack of loops simply requires multiplying this formula by N^2 where N is the number of loops (1). An inductor with spiral geometry has a similar dependence for each loop, but each loop has a different radius as it spirals inwards and therefore a different contribution to the overall inductance of the inductor (1). Besides the inductance of an inductor there are several properties associated with an inductor that determine an inductors behavior within a circuit; such as its effective series resistance (ESR) and quality factor, Q .

The effective series resistance of an inductor is the real resistance of the conductor of which the inductor is composed. This is a property of an inductor that is based on the material of which the conductor is made and the frequency of operation of the inductor. The frequency of operation influences what is known as the skin effect of the inductor, the tendency of a current to flow over the surface of a conductor; As the

frequency of operation of the inductor increases the depth of the skin effect decreases increasing the ESR of the conductor; this relationship is described by the equation below(3).

Equation 2

$$\delta = \sqrt{\frac{2}{\omega\mu\sigma}}$$

In this equation ω represents the frequency of operation in radians per second, δ represents the skin depth, μ the permeability and σ the conductivity. ESR and the self inductance influence the quality factor Q of an inductor.

Equation 3

$$Q = \frac{\omega_0 L}{R} \quad (4)$$

The quality factor is dependent on the frequency of operation ω_0 , the self inductance L and the ESR of the inductor R . This factor is related to the degree with which an inductor generates a magnetic field over losses in the inductor; increased resistance in the inductor increases energy losses and thus the quality of the inductor(5).

An inductor, capacitor and resistor are the fundamental components that can form band-pass and band-reject filters. In the system that will be implemented here both such circuits will be used. A common feature of the behavior of these circuits is the center frequency and the bandwidth over which the circuits operate; these two parameters determine the quality factor, Q of the RLC circuit (6).

Transformers

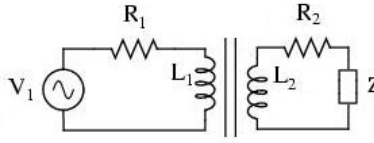


Figure 1: Transformer circuit diagram

An ideal transformer consists of a system of two inductors where each inductor is a part of a separate circuit. The ideal case of a transformer assumes that all of the generated magnetic flux of one coil is directly linked to the secondary coil (6). These circuits are only linked through the coupling of the electromagnetic fields of each inductor, and the behavior of this link follows Faraday's law of induction.

Equation 4

$$M = k\sqrt{L_1 L_2}$$

The mutual inductance is the source of the link between the two coils of the transformer. The mutual inductance, M , represents a factor that determines the degree to which the magnetic flux of one coil is linked to the other coil of the transformer, which is largely dependent on the coupling coefficient, k . The ideal transformer case exists when the coupling coefficient is equal to one. When the primary coil is driven by an AC current this produces an electromagnetic field that produces a current in the secondary coil this effect generates a kind of virtual source in the secondary coil. The current in the secondary coil likewise produces an electromagnetic field and the field linking the coils generates an effective load on the primary coil producing what is known as reflected impedance from the secondary coil. In the case of this system the coupling is not ideal meaning that the coupling coefficient is not equal to one. In fact this factor varies as a function of the geometry of the coils and the relative orientation between the coils. The

impedance associated with the primary circuit is the sum of the impedance associated with each element of the circuit and the impedance of the secondary circuit is found in precisely the same way. Using the diagram of a simple transformer circuit the impedance as seen for each circuit can be described by the equations:

Equation 5: Impedance of the primary circuit

$$Z_{11} = Z_S + R_1 + j\omega L_1$$

Equation 6: Impedance of the secondary circuit

$$Z_{22} = Z_L + R_2 + j\omega L_2$$

These equations combine the impedance for each of the circuits into one term for more efficient analysis. In the first equation Z_S is the impedance of the circuit associated with the source, R_1 is the resistance associated with the inductor, L_1 is the inductance of the primary inductor and ω is the frequency of operation. Similarly the second equation represents the sum of the impedance of all of the secondary circuit elements; the load impedance Z_L , the resistance associated with the inductor and the secondary coil inductance L_2 . An analysis of the voltages in the first and second coils yields the following equations:

Equation 7

$$V_S = Z_{11}I_1 - j\omega MI_2$$

Equation 8

$$0 = -j\omega MI_1 + Z_{22}I_2$$

These equations show that the mutual inductance between the two coils generates a virtual source in the secondary circuit inducing a current in the secondary circuit and a load on the primary circuit. With these two equations an analysis of the transformer will yield the following two equations for the current in each circuit.

Equation 9

$$I_1 = \frac{Z_{22}}{Z_{11}Z_{22} + \omega^2 M^2} V_s$$

Equation 10

$$I_2 = \frac{j\omega M}{Z_{11}Z_{22} + \omega^2 M^2} V_s = \frac{j\omega M}{Z_{22}} I_1$$

These equations show that the current in the second loop is dependent on the mutual inductance between the coils and the current in the primary circuit; greater mutual inductance would lead to higher induced currents in the secondary coil. The current induced in the secondary circuit is completely due to the electromagnetic field produced by the primary coil. Power can be defined by the following equation; where power, P, is associated with the voltage, V, and current, I through a circuit element.

Equation 11

$$P = IV = I^2 R = \frac{V^2}{R}$$

With this equation the power associated with the virtual source is:

Equation 12

$$P = I_2 (j\omega M I_1)$$

I_2 can be rewritten in terms of I_1 :

Equation 13

$$P_2 = \frac{j\omega M I_1}{Z_{22}} (j\omega M I_1) = -\frac{\omega^2 M^2 I_1^2}{Z_{22}}$$

This equation shows that the induced power is proportional to the induced voltage squared divided by the impedance of the secondary circuit. The power delivered by the primary circuit is equivalent to the power absorbed in by the mutual inductance of the two coils as shown by the equation below which is the power absorbed by the reflected impedance in the primary circuit.

Equation 14

$$P_1 = (j\omega MI_2)I_1 = -\frac{\omega^2 M^2 I_1^2}{Z_{22}}$$

Class E Power Amplifier

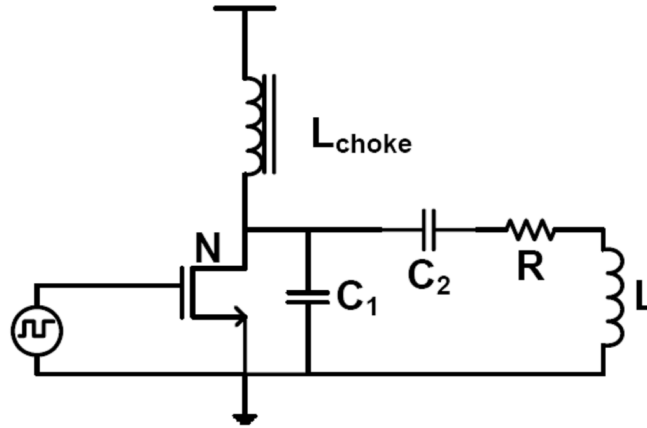


Figure 2: Simple class E power amplifier schematic.

The class E power amplifier is a circuit developed by Nathan Sokol that would theoretically have 100% efficiency(7). A circuit diagram of the class E power amplifier proposed by Nathan Sokal appears above. The transistor in this circuit acts as a switch that either shorts or allows current to flow through the capacitor C1. The circuit is designed to provide the desired output power while minimizing the power dissipated within the circuit; for example power is minimized through the transistor by not allowing a current and voltage across the transistor at the same time.

The design equations for the class E power amplifier have been defined in other research. The function of the class E power amplifier like all implements circuits is subject to fluctuations from its theoretical behavior due to the variability of actual component values. The quality factor of the inductor has a great influence on the output power of the class E power amplifier (7). There is an explicit set of design equations

developed by Sokal by fitting data of the actual function of the circuit, these equations are as follows:

$$C1 = \frac{1}{2\pi f R \left(\frac{\pi^2}{4} + 1 \right) \frac{\pi}{2}} \left(0.99866 + \frac{0.91424}{Q_L} - \frac{1.03175}{Q_L^2} \right) + \frac{0.6}{(2\pi f)^2 L I}$$

$$C1 = \frac{1}{34.2219 f R} \left(0.99866 + \frac{0.91424}{Q_L} - \frac{1.03175}{Q_L^2} \right) + \frac{0.6}{(2\pi f)^2 L I}$$

$$C2 = \frac{1}{2\pi f R} \left(\frac{1}{Q_L - 0.104823} \right) \left(1.00121 + \frac{1.01468}{Q_L - 1.7879} \right) - \frac{0.2}{(2\pi f)^2 L I}$$

Figure 3: Design equations for a class E power amplifier developed by Sokal.

In these equations the first two equations describe a curve that determines the value of C1 and the third describes the value of C2 in the in the diagram of a class E power amplifier above. Using the diagram of the circuit above the value C1 and C2 are dependent upon the quality factor of the inductor L, the inductance of the RF choke inductor, the load resistance R and the frequency of operation f . The value of L2 according to Sokal is a designer's choice, but has a specific relationship with Q_L and R described by the equation:

Equation 15

$$L2 = \frac{Q_L R}{2\pi f}$$

The output power of the class E power amplifier is dependent on both the supplied voltage and to some degree the value of Q_L according to the equation from fitted data developed by Sokal(7).

Equation 16

$$P = \left(\frac{V_{cc} - V_o}{R} \right) 0.576801 \left(1.0000086 - \frac{0.414395}{Q_L} - \frac{0.577501}{Q_L^2} + \frac{0.205967}{Q_L^3} \right)$$

In this equation V_{cc} is the value of the supply voltage and V_o is the value of the transistor saturation offset voltage.

Rectifier Circuits

Any sinusoidal or oscillating signal that has an average value of 0 has no zero frequency component and therefore has no DC power. A simple nonlinear circuit that changes an oscillating signal with zero DC component to a signal with nonzero DC component is a simple half wave rectifier; the circuit is depicted here.

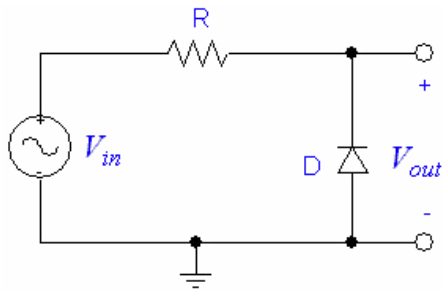


Figure 4: Diagram of a half wave rectifier

This circuit consists of a diode and a resistor. When the potential difference across the diode is great enough to switch the diode from an open operating mode to a conducting mode it will let a current pass through the resistor. The diode acts as an open circuit when reverse biased. If an AC signal is applied, such as a sinusoid, this circuit effectively deletes one half cycle producing a one sided output signal since one half of the circuit will forward bias the diode and the other half will reverse bias the diode. This one sided output signal no longer has an average value of zero and thus a DC component can be extracted from this signal.

Radio Frequency Tissue interactions

The system that is being developed in this investigation is meant to have possible applications as a wireless link for biomedical devices such as a wireless transcutaneous link. As such the effects of the electromagnetic field generated by the coils on the tissue must be considered. Not all radio frequencies are able to pass through tissue effectively. The table below shows as the frequency of the radio frequency radiation increases the penetration depth in the tissue decreases. A transmitter that functions at lower frequencies would be able to transmit further in tissue. There is also another limitation on the range of frequencies available for use in wireless communication systems. The federal Communications Commission (FCC) designates specific frequency bands for predetermined usage, which includes scientific and medical purposes. The FCC allows operation within the ISM bands for industrial, scientific or medical use, of these specific frequency ranges one of them is 13.56MHz(8). This frequency band is low enough to allow for sufficient penetration for applications of interest to the system that is developed here.

Table 1: Dielectric Parameters for muscle tissue at various frequencies (9).

Frequency (MHz)	Relative Dielectric Constant	Conductivity (S/m)	Penetration Depth (cm)
0.1	1850	0.56	213
1	411	0.59	70
10	131	0.68	13.2
100	79	0.81	7.7
1000	60	1.33	3.4
10000	42	13.3	0.27
100000	8	60	0.03

Since this investigation is focused on designing a system intended for biomedical applications there are safety standards for this design that must be considered.

Electromagnetic radiation is non-ionizing and so the thermal effects of electromagnetic radiation on tissues are of a major concern since overheating can cause damage to the tissue. The amount of exposure to RF radiation is quantified by the average rate of energy absorption for a particular mass (9). This quantity is known as the specific absorption rate (SAR). The spatial peak SAR in a controlled environment should not exceed 8W/kg over any 1 gram of tissue according to IEEE standard C95.1(10).

Silk Polymer Overview

Silk is a protein polymer produced by insects, *bombyx mori*, which in its natural state contains two proteins sericin and fibroin (11). Sericin acts like a binder that holds fibroin fibers together. In its processed aqueous state the sericin is removed leaving an aqueous solution of fibroin. The transition between a silk solution and silk gel occurs when the coiled nature of the protein switches to a β -pleated sheet formation which is less soluble than its previous conformation (11)(12). The amino acid structure of fibroin is dominated by alanine, glycine and serine, these amino acids form β -pleated sheet formations within the secondary structure of fibroin (11). The formation of silk polymers in natural settings is largely unknown due to the complex nature, of both the mechanical and chemical composition, of the glands in the insects that produce silk.

Aqueous solutions of silk fibroin from *bombyx mori* have been shown to form silk gels under certain conditions. In some studies the formation of a silk gel is affected by temperature, calcium ion concentration, pH and poly(ethylene oxide) (PEO)(11). More recently at Tufts University methods of producing silk gels using externally applied electric fields have been studied as another method of producing silk gels. It was observed that an applied static electric field appeared to cause an aqueous silk solution to

gel on an electrode (13). The figure below shows an example of one of the experiments performed with a silk solution and a static electric field.



Figure 5: Picture of petri dish with electrode setup showing gel formation.

Methods

System Overview

The system that was developed for this project consisted of two main components a transmitter and a receiver. The transmitter consists of a class E power amplifier whose inductor of the resonant circuit is the transmitter coil. The receiver is an LC tank and a rectifier circuit. As depicted below, information from the transmitter and receiver systems will mainly consist of information that can be gathered through an oscilloscope. The diagram below depicts the general setup of the system that was implemented in this work.

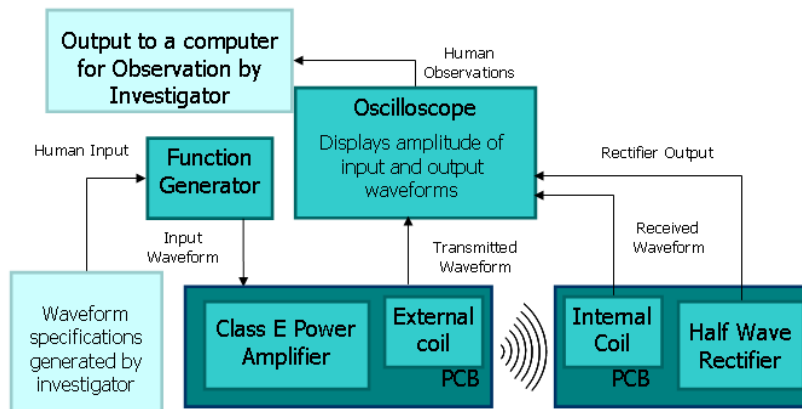


Figure 6: System diagram depicting the full system

Coil Design

There are closed form equations for simple conductor geometries that are used to design antennas; such as a close form expression for the self inductance of a loop of wire. A circle is a special case that contains symmetry that simplifies the analysis of the conductor whereas when geometries deviate from the ideal situation models of these conductor geometries become cumbersome; for the coils used in this system an octagonal shape was chosen to satisfy concerns about the manufacturing process of printed circuit boards. Multilayered octagonal spiral shaped inductors have a more complex geometry and less symmetry than circular spirals. Closed form approximations of electrical characteristics of complex coil geometries are mathematically intensive and difficult to derive. Maximizing parameters for energy transfer between coils using these equations for the purpose of developing new coil geometries further complicates these methods. Therefore a numerical approach was used to find an energy efficient design.

Designing the coils that were used for this system developed here began with simulating their electrical characteristics in FastHenry. FastHenry is a software program developed at MIT to model electrical properties of conductors with a specific geometry. In order to model conductors using FastHenry, the program requires a description of the conductor material, geometry and simulation parameters in the form of an input file. Writing an input file for specific coil geometries individually would have been computationally intensive and slow. VBA code was developed to alleviate this time constraint. Two programs were developed for this project. One VBA script models individual coil geometries while the other models coil pairs with varying orientations between the coils. The code that models coil pair writes the required input file for

FastHenry that models any orientation and separation between the two coils. Specified coil geometries are entered into the program in a spreadsheet format. The VBA script reads the spreadsheet and generates the specified coil geometry. Images of each spreadsheet program show the precise format that these parameters are listed; these images appear in the Appendix. Modeling conductor geometries faster and more efficiently was vital to developing a conductor design that was used in the final system.

There are several methods described in literature that iteratively determine an energy efficient transmitter and receiver coil geometry. One such iterative method described by Reinhold *et. al.* focuses on optimizing the coupling coefficient between the coils to enhance power transmission. Increasing the coupling coefficient between the coils increases the effect that the generated electromagnetic field has on the receiver coil increasing the generated current and thus increasing the transferred power. This process begins with making several operating assumptions about how the coils are going to be oriented with respect to one another and used in the system.

In biomedical applications where this coil design could be used in implantable device applications a maximum receiver diameter was set to 1cm to align with previously held standards for implantable devices (14). Biocompatibility is a concern when designing devices that might be used within a living system. Biocompatibility concerns not only the shape of the implant but also the material it is composed. FR4 is the material that most PCBs are composed of, which in of itself is not the most biocompatible material. It will be used here to demonstrate the transmission characteristics of the coils under laboratory conditions. The other operational criterion was that maximally the two coils were going to be held up to 2cm apart.

As described by processes like the ones presented by Reinhold *et. al.* and Kendir *et. al.* the next step was to define base turns of each conductor(3, 15). Defining these base turns required defining the physical constraints on the coils. For the intended implantable coil this lead to a maximum diameter of 1cm. A base turn of 1cm was chosen for this coil since the greater the surface area exposed to the magnetic field means that a greater amount of electromagnetic flux can be captured and thus a greater current can be generated with a given electromagnetic field. Next the base turn of the transmitter coil needed to be determined. This was done by finding the radius and track width that maximized the coupling between the two base turns of the coils. Following this the optimum number of turns for the primary coil was found by varying the number of turns and examining the effect that this factor had on the coupling coefficient between the primary inductor and the base turn of the secondary inductor. These steps determined the geometry for the primary inductor. To find a design for the secondary inductor the process just described was turned around and the parameters of the secondary coil were varied and the coupling was simulated with the base turn of the primary coil. The parameters of the secondary coil that produced the greatest coupling with the base turn of the primary coil were chosen for the final coil design.

Coil Simulations

The series of steps described above were followed here. In accordance with the first step the base turn of receiver coil was set to a radius of 1cm in order to maximize the net magnetic flux through the receiver coil. With this base turn for the receiver the base turn diameter for the transmitter was determined by finding the radius of the coil that maximized the coupling coefficient between the two turns alone. The receiver coil had a

diameter of 1cm and a track width of .3mm. The choice of .3mm was arbitrary and will be adjusted in a later step. The results of varying the track width and diameter of the base turn of the transmitter coil are shown from two different points of view below. The Surface representation shows more clearly how trace width and the diameter of the transmitter coil effects the coiling coefficient between base turns of the coils. The coils are centered with respect to one another and are simulated to be 2cm apart.

Coupling Between Base Coil Turns with Variations of the Transmitter Coil Turn Paramters

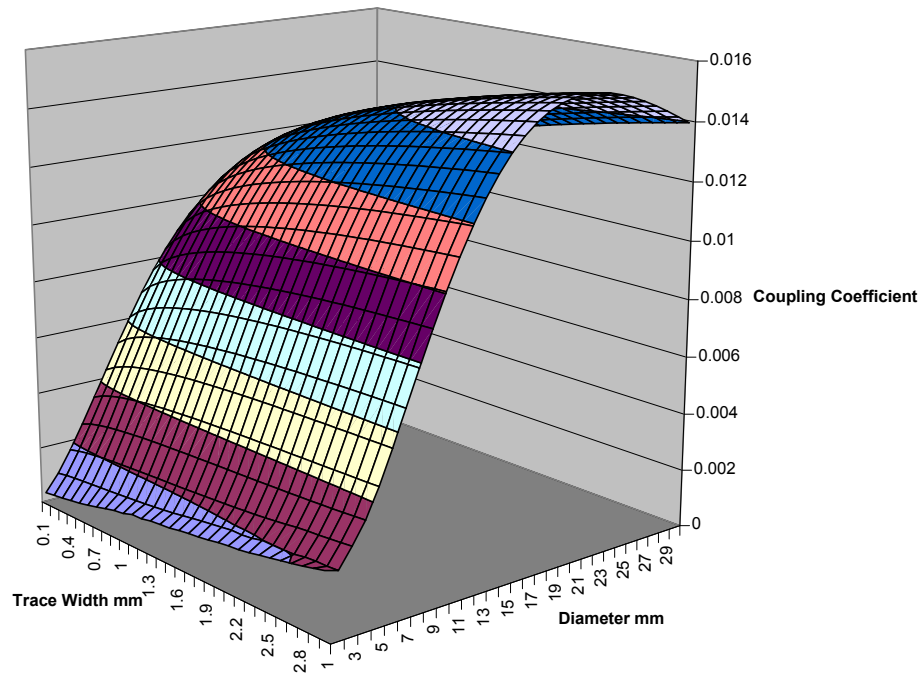


Figure 7: Graph depicting effect of variation in transmitter coil parameters.

While the surface view is useful for observing how the coupling coefficient changes as transmitter coil parameters are varied it is less clear what the optimal coil diameter might be. For this reason a second graph was made that suppresses the trace width axis and displays for each trace width only the effect of the diameter of the coil on the coupling coefficient. With this graph there appears to be a clear peak that occurs with a coil radius of 20mm. The other coil parameter that these two graphs help determine is

the coil trace width, as both graphs show as the coil trace width increases the coupling coefficient between the base coil turns increases.

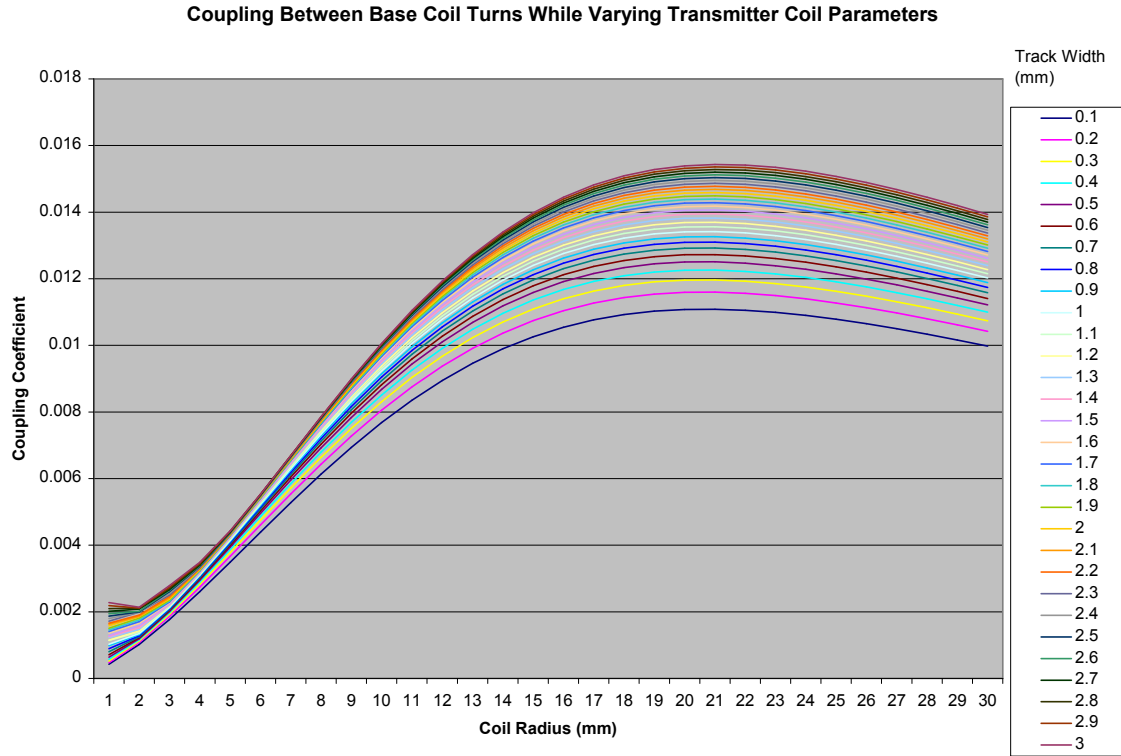


Figure 8: Depiction of an alternative view of varying transmitter coil dimensions.

The effect of track width on coupling decreases with increased coil diameter; a track width of 1.5mm was chosen to increase the number of turns that would fit in to one layer of the coil and take advantage of the effect of increased track width on the coupling coefficient.

The next simulation shows the effect of increasing the number of turns of the transmitter and the coupling with the base turn of the receiver coil. As the graph shows that as the number of turns increases the coupling between the two coils increases and reaches a peak. The peak represents the optimal number of turns for the transmitter coil.

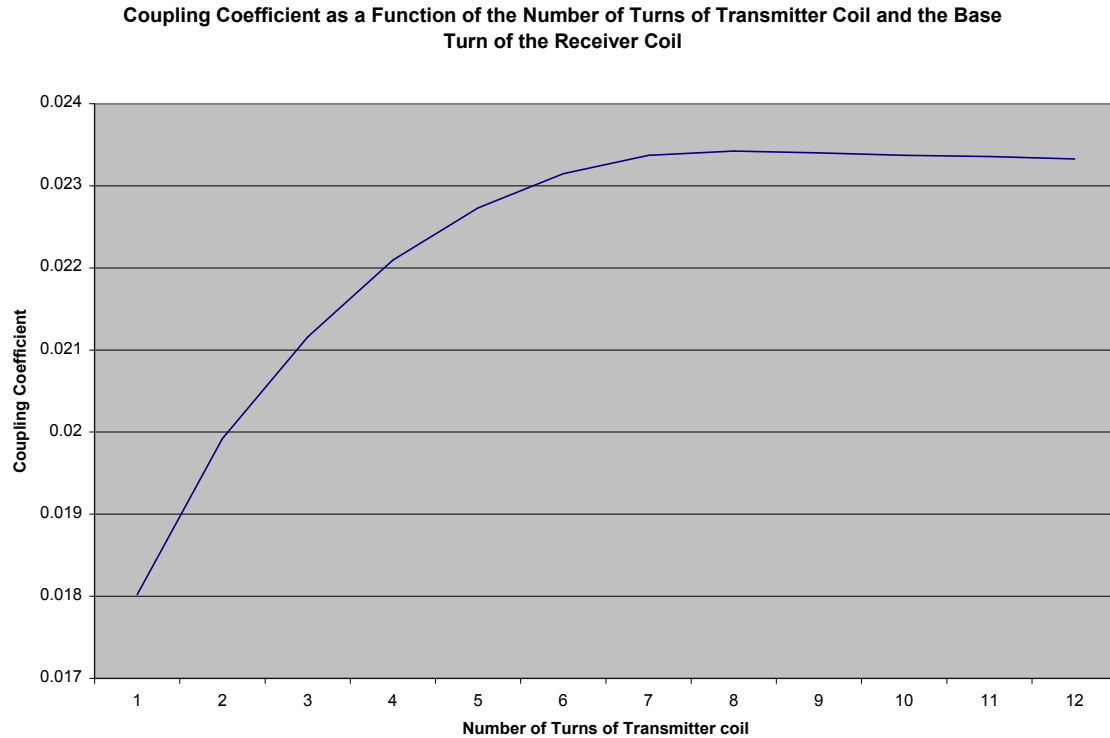


Figure 9: A graph depicting variations in the coupling coefficient due to the number of turns of the transmitter.

The number of turns determined for maximum coupling with the base turn of the receiver coil was determined from the graph above to be eight turns. The transmitter coil parameters have now been determined for maximum coupling with the base turn of the receiver coil. The focus of the simulations will now be on the receiver coil parameters with respect to the base transmitter coil turn. The final parameters of the transmitter coil appear in a summary table below.

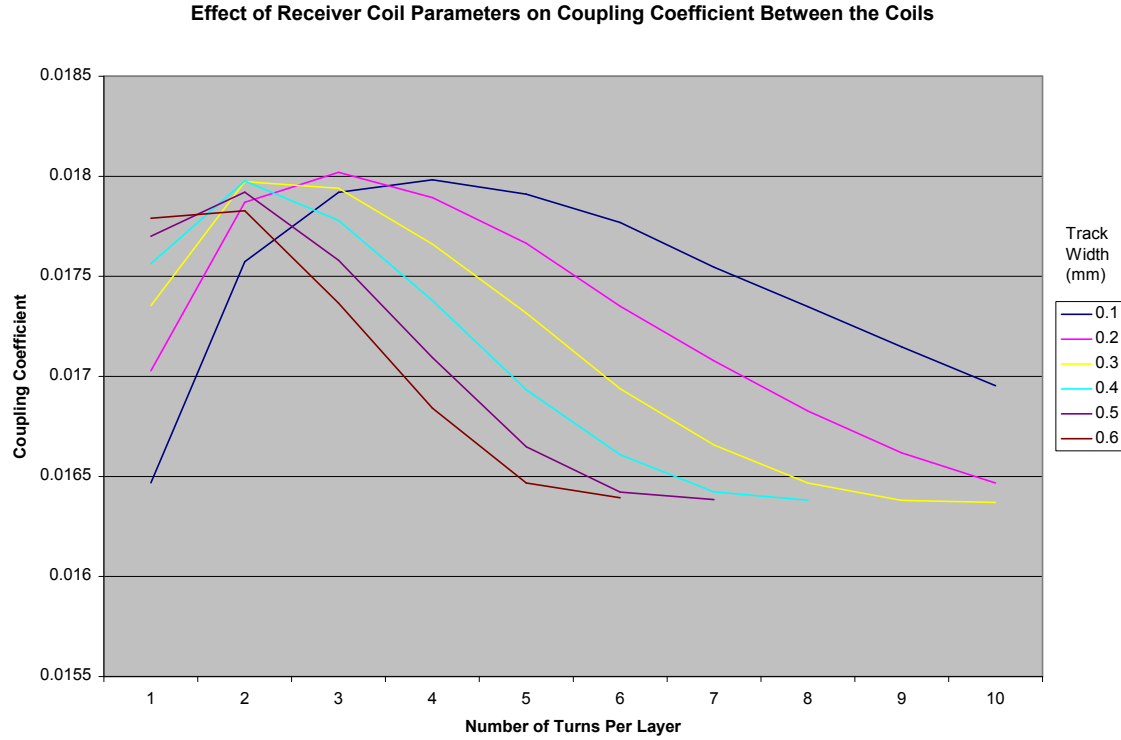


Figure 10: Receiver coil parameters on coupling coefficient

This graph shows the effect of varying receiver coil parameters on the coupling coefficient between the two coils at a distance of 2cm. In this simulation both track width and the number of turns in each layer of the coil is varied. PCBs are capable of supporting multiple layers, as the spiral geometry is flat and printed within one layer multiple layers can be stacked to increase the inductance of the coil without adversely affecting the required volume of the coil. The simulation above was performed multiple times varying the number of coil layers for the receiver coil. It was found that increasing the number of coil layers increases the coupling coefficient between the transmitter and receiver coils, but for the PCB designed here a PCB with two layers was used. As the graph shows for a two layered receiver coil a track width of .2mm and 3 turns for each layer yields the greatest coupling coefficient between the coils.

Final Coil Design

From the simulations conducted above the final coil parameters are as they appear in the table below. After completing these simulations three other simulations of the coil pair were conducted to examine the characteristics of these coils as they would appear in the system.

Table 2: Final coil design parameters

	Maximum Radius	Turns per Layer	Track Width	Number of Layers
Transmitter Coil	2cm	8	1.5mm	1
Receiver Coil	.5cm	3	.2mm	2

FastHenry also provides information about the inductance, ESR and Q of the inductors. These characteristics of the inductors predicted by FastHenry are listed in the table below.

Table 3: FastHenry estimates of inductance, series resistance and Q

	Inductance (nH)	Q_L	ESR (Ω)
Transmitter	1504	605.3	0.412
Receiver	384	79.3	0.212

The first simulation examines the effect of rotating the receiver coil through 180 degrees and examining the coupling coefficient between the two coils. As expected the highest coupling coefficient occurs when the two coils are parallel to one another and the lowest coupling occurs when the coils are perpendicular to each other.

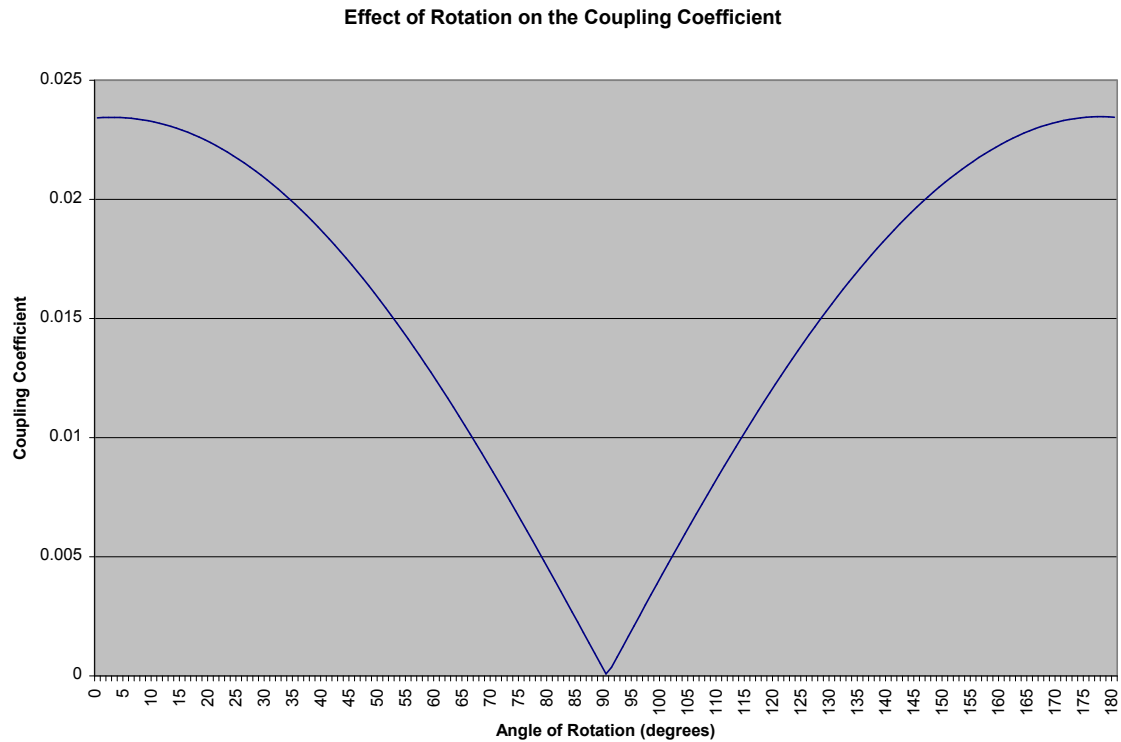


Figure 11: Effects of rotating coils in space and the effect on coupling.

The next simulation shows the effect of moving the coils parallel to each other over one sector of the xy plane while maintaining a constant separation of 2cm between the coil pair. As the graph shows the highest coupling occurs when the two coils are centered and parallel and coupling decreases as the coils become further off center from one another.

Coupling Coefficient Over a Sector of the XY Plane with a Constant Separation of 2 cm

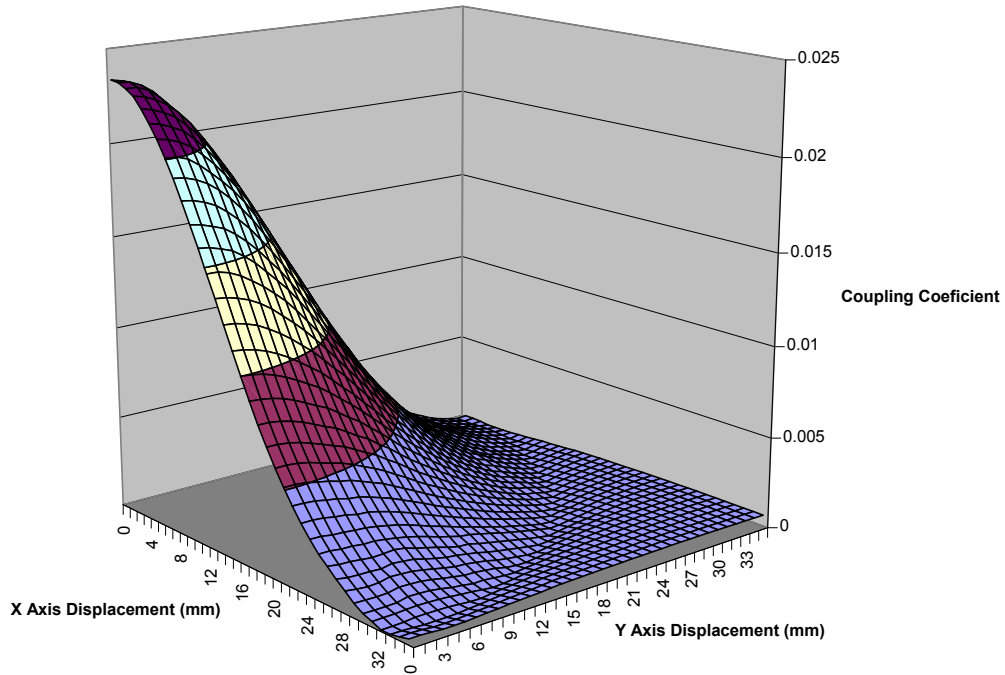


Figure 12: Variation in coupling over xy plane.

The last graph shows the variation in coupling as the two coils are moved away from each other along the z axis. The two coils are always centered in this simulation. As expected the highest coupling occurs when the two coils are closest together. There is a significant drop of in coupling as the coils are moved away from each other.

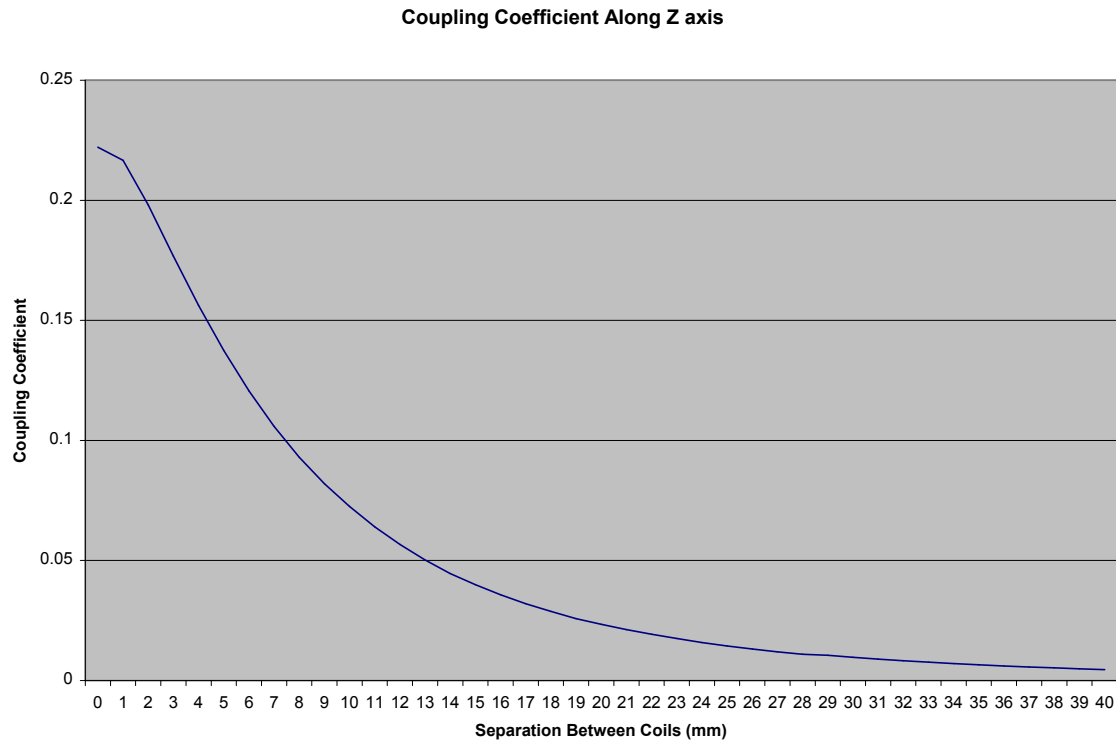


Figure 13: Graph showing the simulated variation in coupling coefficient along the z axis

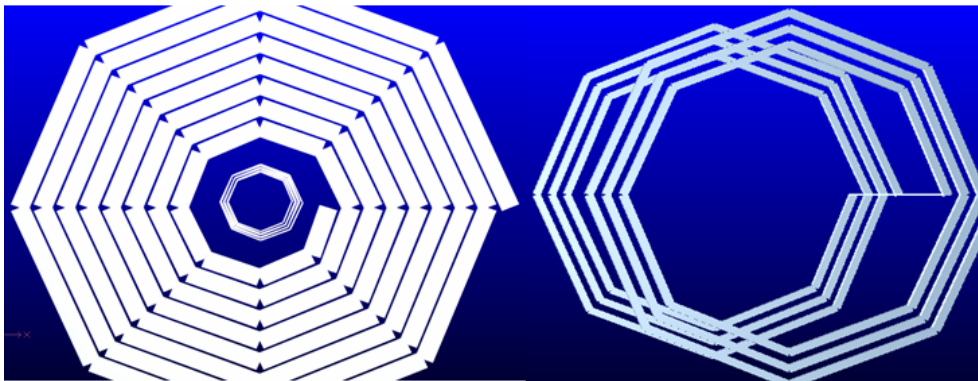


Figure 14: FastHenry depiction of coils

These are FastHenry images of the coils used in the final system. This figure portrays coil modeled together, left, and a secondary coil modeled individually, right.

Radio Frequency Safety Calculations

The maximum exposure to RF radiation allowed by IEEE regulations is 8mW/gram over any 1 gram of tissue for local exposure. This system largely relies on

near field effects of the electromagnetic field generated by the primary coil. The intensity of the near field EM radiation decreases rapidly with distance so the effects of the field are limited to a small area around the coil. As the graph below shows the area exposed to the greatest intensity is the area enclosing the transmitter coil including the area immediately beyond the coil. This increases the exposed area to include not only the coil but also the area approximately .5cm around the coil making the exposed area approximately 17.7cm^2 . This area is the tissue directly exposed to the field so the exposed volume is 17.7cm^3 . Assuming that tissue has a similar density to water 17.7g of tissue is exposed to the EM field. With this value the maximum allowable amount of power absorbed by the tissue is the product of the maximum SAR and the exposed area or 141.4mW.

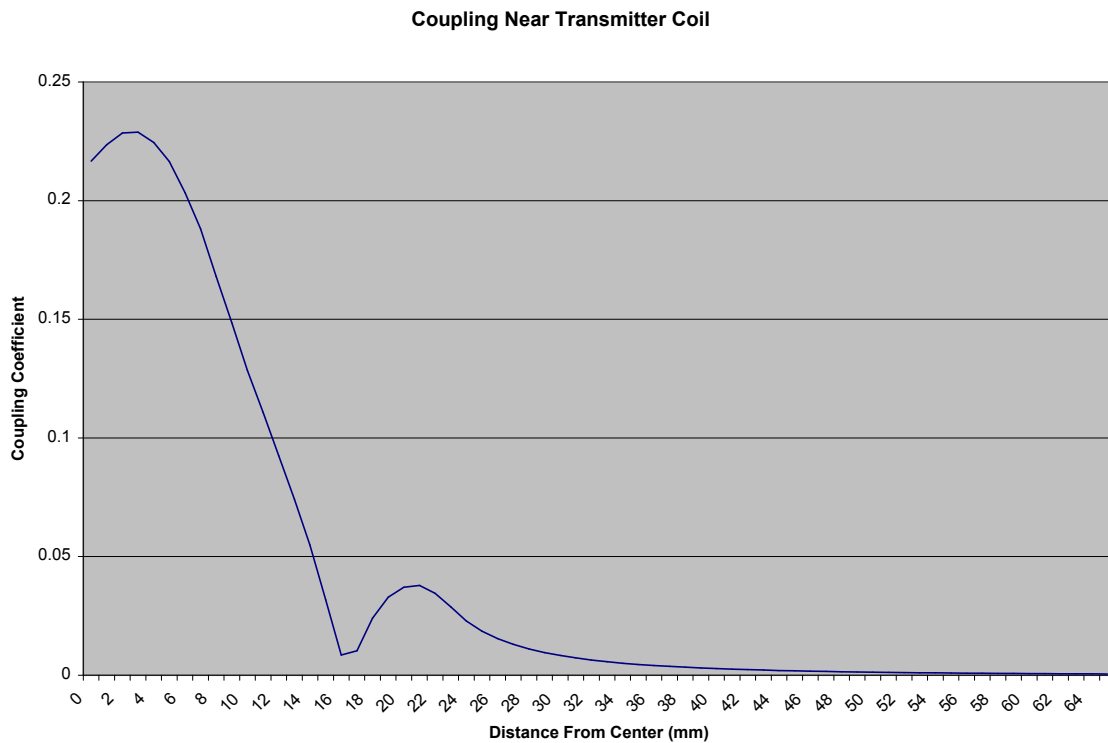


Figure 15: Coupling coefficient between the final coils along a line outward from the center of the transmitter with 1mm separation between the coils.

Class E Power amplifier design

The design equations described earlier were equations fitted to data about class E power amplifiers. Design equations can also be derived from the circuit diagram itself.

This derivation has been shown in previous research; the results of this analysis are reproduced here(16):

Equation 17

$$C1 = \frac{1}{\omega R 5.4454}$$

Equation 18

$$C2 = \frac{1}{\omega R (Q_L - 1.1524)}$$

Equation 19

$$L2 = \frac{Q_L R}{2\pi f}$$

The coil design section discussed two coil geometries for transmitted and receiver that were designed to be used in the system. The transmitter coil in this system acts as the inductor L2 in the class E power amplifier. The discussion about the coil design yielded specific simulated values for the transmitter inductor. These values help provide values for Q_L and R that aid in the calculation of C1 and C2. However comparing the simulated value of Q for the transmitter inductor versus the measured value yields a very different value for Q. Since the values of Q presented had such a great difference yet the value of inductance agreed in both the simulation and the measured value, the measured value of Q was used to find R to determine the value of C1.

Value of R

$$R = \frac{(L2)2\pi f}{Q_L} = \frac{(1504 \times 10^{-9})2\pi(13.56 \times 10^6)}{23} = 5.57\Omega$$

The value of C1

$$C1 = \frac{1}{2\pi R 5.4454} = \frac{1}{2\pi (13.56 \times 10^6)(5.57)(5.4454)} = 387 \text{ pF}$$

The value of C2

$$C2 = \frac{1}{\omega R (Q_L - 1.1524)} = \frac{1}{(2\pi 13.56 \times 10^6)(5.57)(23 - 1.1524)} = 96.45 \text{ pF}$$

The output power of the class E power amplifier is directly dependent on the supply voltage to the amplifier and the load resistance R. Since this investigation is mainly interested in the transmission characteristics of the coils and not necessarily a specific transmitted power the selection of input voltage and output power was in accordance with previous research for implant applications. Zhenying Luo's thesis on wireless systems chose a supply voltage of 7.5V for a target output power of 4.5W so this work also chose these target values. The supply voltage was calculated using a modified version of the equation for the output power described in the background section that neglects the effect of the inductor Q.

Equation 20

$$P = \left(\frac{V_{cc} - V_o}{R} \right) 0.576801$$

In this equation V_o is the saturation voltage of the transistor when it is conducting and V_{CC} is the supply voltage. With a target output power of 4.5W the above equation yields approximately 7.5V for the circuit supply voltage.

Receiver Tuning Calculations

In order to form a tuned tank with the transmitter circuit the LC tank of the receiver must be tuned to the same frequency. This is accomplished simply by using the relationship for the resonant frequency of an LC circuit.

Resonant frequency of an LC tank:

Equation 21

$$\omega = \frac{1}{\sqrt{LC}}$$

Calculated capacitor value for receiver LC tank:

Equation 22

$$C = \frac{1}{\omega^2 L} = \frac{1}{(2\pi 13.56 \times 10^6 \text{ Hz})(383 \times 10^{-9})} = 359.7 \text{ pF}$$

Summary of System Parameters

The following tables summarize the component parameters used in the circuits. Some of the discrete component values such as those for the capacitors of the systems were implemented with a series of capacitors in parallel to approximate the calculated value.

Table 4: Table showing system component parameters

Transmitter Parameters

Supply Voltage	7.5V
Frequency of Operation	13.56 MHz
L1 Inductance	1504 nH
C1Capacitance	387 pF
C2 Capacitance	96.45 pF
Transistor Gate Voltage	13.56mHz, 8Vpp Sine wave

Receiver Parameters

L1 Inductance	384 nH
C1 Capacitance	359.7 pF

Experimental Measurements

Experimental Verification of Coil Behavior

FastHenry was able to simulate the inductive characteristics of the coils both individually and in pairs. The characteristics that were simulated individually were then compared to experimentally measured values of these parameters. The values that were measured were inductance, ESR and Q.

As derived earlier the power transferred to the secondary circuit in the transformer should look like the following equation, which reappears in the first half of equation 25. In this experiment the receiver is just a simple LC tank so Z_{22} has the following form.

Equation 23

$$Z_{22} = R_2 + j\omega L_2 + \frac{1}{j\omega C}$$

From Ohm's Law the relationship between current and voltage allows I_1 to be rewritten in terms of the voltage and impedance of the primary inductor yielding the following relationship.

Equation 24

$$I_1 = \frac{V_1}{j\omega L_1}$$

With these two relationships the power in the secondary coil can be rewritten in terms of the primary inductance and the voltage across the inductor.

Equation 25

$$P_2 = -\frac{\omega^2 M^2 I_1^2}{Z_{22}} = -\frac{\omega^2 M^2 \left(\frac{V_1}{j\omega L_1} \right)^2}{R_2 + j\omega L_2 + \frac{1}{j\omega C}} = \frac{M^2 V_1^2}{L_1^2 \left(R_2 + j\omega L_2 + \frac{1}{j\omega C} \right)}$$

Using the relationship between the coupling coefficient and the mutual inductance between the two coils this relationship can be rewritten to find the coupling coefficient between the two coils as a function of the primary inductor parameters and the received power.

Equation 26

$$k = \frac{P_2 L_1 \left(R_2 + j\omega L_2 + \frac{1}{j\omega C} \right)}{L_2 V_1^2}$$

This equation relates the measured parameters of the system with the coupling coefficient between the coils. This permits a comparison between the simulated coil characteristics and the experimental measurements. Two experiments will be performed to examine the coupling characteristics of the designed coils. The first will examine how the coupling varies between the coils when the receiver coil is moved away from the primary coil when both coils have the same central axis. The second experiment will examine the effect of turning one coil in relation to the other and examining how the coupling changes as a function of the number of degrees the receiver coil is off from being parallel with the transmitter.

Novel Experiments

Two experiments with the transmitter and receiver coils were performed to demonstrate a novel use of wireless power transmission. These experiments explored methods of remotely inducing silk to form a gel.

The first silk experiment looked at directly gelling silk using direct exposure to the electromagnetic field of the transmitter coil. In this experiment a petri dish containing

2.5 – 3ml of 8% one month old silk solution was placed directly on top of the transmitter for a period of 1 and a half hours. The petri dishes were then allowed to sit out in the covered unsealed petri dishes in the lab until gelling occurred. The petri dish that was exposed to the electromagnetic field was compared to a petri dish that was unexposed. Both dishes were left out in the lab for the same amount of time.

The second experiment used a half-wave rectified signal generated by the receiver to produce a polar electric field where one electrode was always more positive than the other. In this experiment two petri dishes were prepared that contained 2.5mL of the same aqueous silk solution that was 6 days old and had a concentration of 7.7%.

Results

Experimental Coil Measurements

Individual Coil Parameters:

The table below represents the data initially collected about the coils themselves using an RLC meter. The RLC meter was measuring the values for each inductor at 10MHz. The values collected here were compared to the simulated values generated using FastHenry.

Table 5: Experimentally determined values of inductors

	Inductance nH	Series Resistance Ohm	Quality Factor
Transmitter	1496.7	5.4	23.0
Receiver	417.9	2.5	15.7

Table 6: Table comparing simulated and experimental values of designed coils

	Simulated	Experimental	Percent Error (%)
Transmitter Inductance (nH)	1504	1496.7	-0.485
Transmitter Series Resistance (Ω)	0.412	5.4	1210.680
Transmitter Q	605.3	23	-96.200
Receiver Inductance (nH)	384	417.9	8.828
Receiver Series Resistance (Ω)	0.212	2.5	1079.245
Receiver Q	79.3	15.7	-80.202

These results show the differences between the simulated and experimentally measured values for the inductors by themselves.

Amplifier Output Power:

In order to measure the output power of the class E power amplifier the circuit needs to be modeled as its Thevenin equivalent to determine the output impedance of the circuit. The output power of the class E amplifier will be the open circuit output power of the Thevenin equivalent. Since the Thevenin equivalent is being used to determine the output impedance two measurements were made one with a resistor was put across the inductor and one without. These two measurements represent the loaded output voltage and the open circuit output voltage of the class E power amplifier. Using Ohm's law the difference in voltages and the known value of the added resistors determines the Thevenin resistance associated with the class E power amplifier.

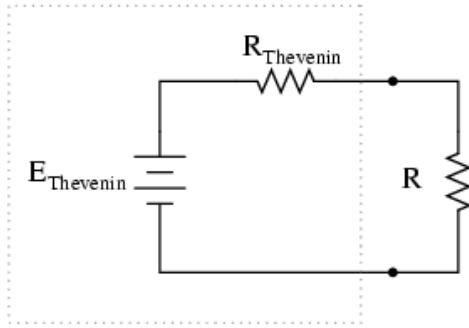


Figure 16: Diagram of Thevenin equivalent circuit with load.

Output Impedance of Class E Power Amplifier

Resistor used: 98.5Ω

Open circuit voltage (V_{p-p} across Inductor): $50.9V$

Voltage with Load (V_{p-p} across Inductor): $4.89V$

Estimated output impedance: 926.8Ω

Output Power without receiver coil

$$P = \frac{V_{RMS}^2}{R} = \frac{\left(\frac{V_{pp}}{2\sqrt{2}}\right)^2}{R} = \frac{17.99^2}{926.8} = 349.4mW$$

Received Power:

In the case of the receiver the presence of the electromagnetic field acts as a virtual source that induces a current in the circuit. If this is the case then all of the power in the circuit elements of the receiver will equal the power received. A similar calculation that was done with the class E power amplifier was done with the receiver to find the receiver to calculate the received power.

Receiver Thevenin Resistance:

(Minimal separation between transmitter and receiver was maintained to make these measurements)

R used: 51.2Ω

Open circuit voltage (V_{p-p} across receiver): 8.485V

Voltage with Load(V_{p-p} across receiver): 5.2V

Estimated output impedance: 32.3Ω

Receiver Power calculation:

The received power varies with distance and orientation. These aspects of the transmission between transmitter and receiver will be investigated next. The calculation below represents the received power with minimal separation and the transmitter is set as it was to make the calculation of impedance.

$$P = \frac{V_{RMS}^2}{R} = \frac{\left(\frac{V_{pp}}{2\sqrt{2}} \right)^2}{R} = \frac{3^2}{32.345} = 278.2mW$$

Measured and Simulated Transmission Characteristics:

Using the estimated impedance for the receiver to calculate the power, the equation derived earlier relating the coupling coefficient to the circuit parameters was used to generate the following graphs to relate the experimental and simulated coupling coefficients. During this experiment the two coils were kept parallel and with the same center and moved outward from each other.

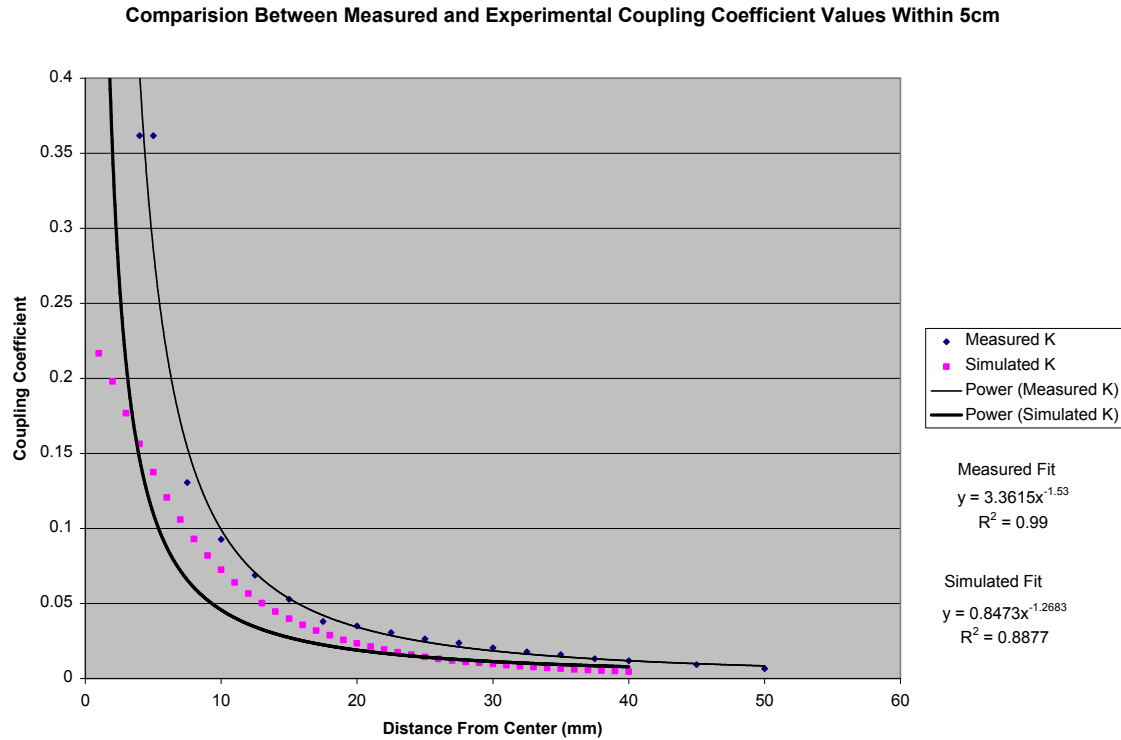


Figure 17: Measured and Simulated values of coupling coefficient as a function of separation close to coils.

The graph above examines the coupling between the two coils within 5cm of each other. This was done to examine the change in the coupling when the two coils are near each other, as the greatest changes in coupling occur in this area. Both the experimental and simulated data are fitted to examine the possible dependence of the coupling between the coils in this region as a function of distance. Experimentally the curve shows a -1.53 power dependence versus the -1.27 dependence on distance in the simulated data.

The next graph displays a log-log plot of the data for the entire measured range from 0 to 19cm. This graph displays some visual information on how well the trends in the measured and simulated results correspond with one another overall.

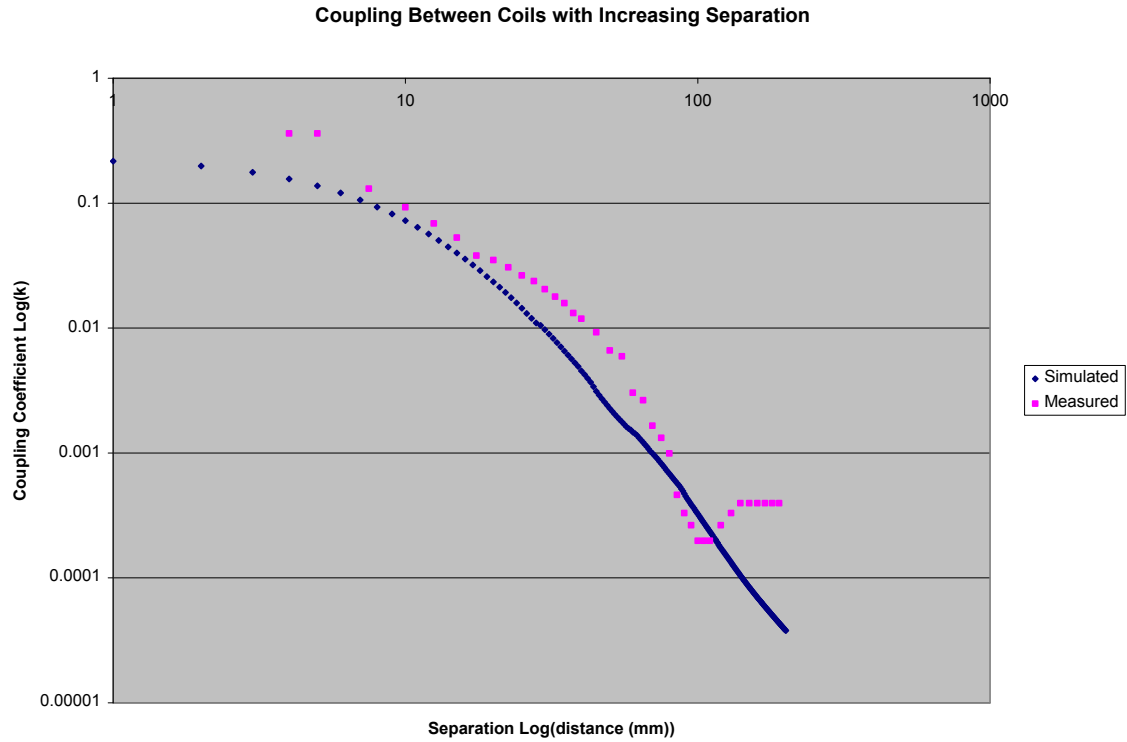


Figure 18: Log-log plot of the effect of separation between coils on the coupling coefficient for the measured range of 0-19 cm.

The next graph displays the same data as the previous graph on a linear scale. Here both simulated and measured data sets were fitted with a power trend to compare the dependence of each data set on the separation between them. Similar to the graph that compares the coupling between the coils within 5 cm the dependence of the coupling between the coils with distance appears to correspond to similar values; the measured power dependence is -2.2 and the simulated dependence with distance is -2.34.

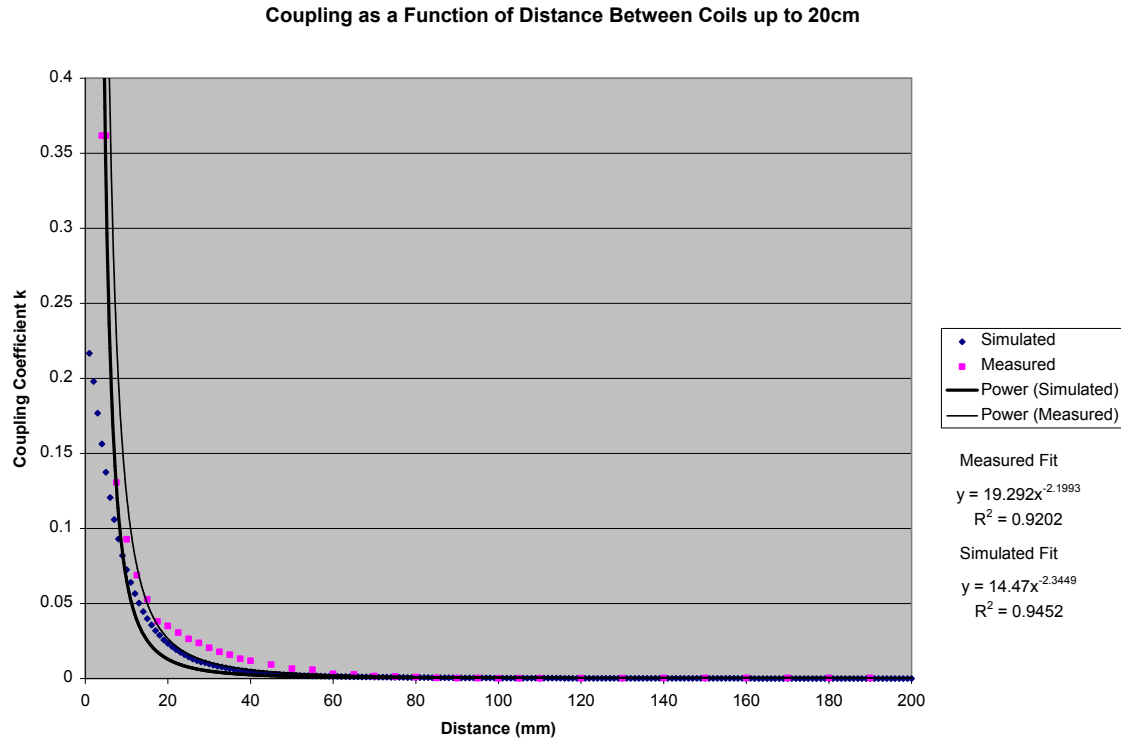


Figure 19: Plot of all measured and simulated data for coupling as a function of distance.

The next graph shows a comparison between simulated and measured values of the coupling coefficient when the coils are rotated a certain degree with respect to each other. A trend line was not fitted with this data since upon visual inspection there is clearly a very different trend between the simulated and experimental results, these aspects of this second experiment will be discussed in the analysis and discussion sections.

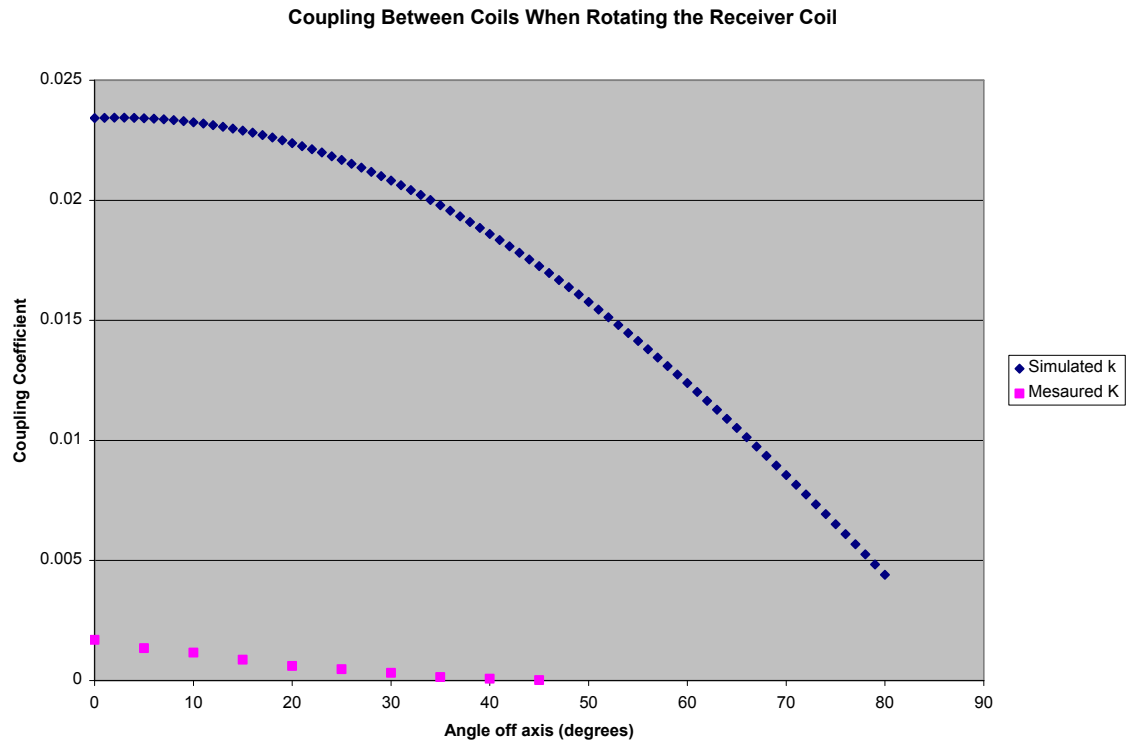


Figure 20: Comparison of coupling when coils are rotated with respect to each other.

Silk Experiment Results

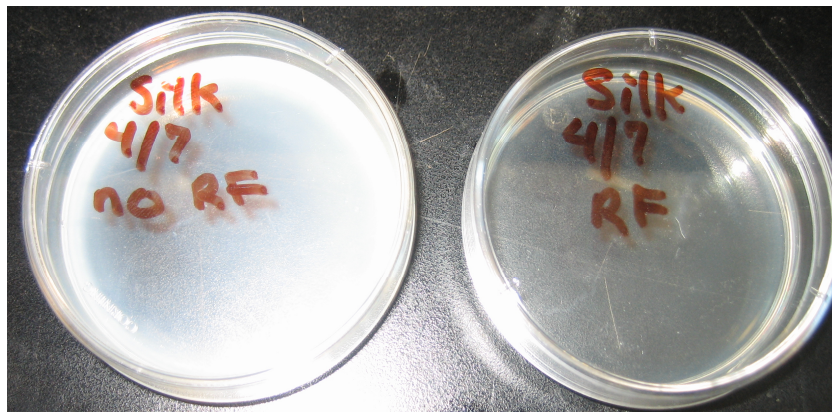


Figure 21: Image showing degree of gel formation in the silk after a week.

The figure above shows that there were differential gelling times between the two samples. The RF exposed sample remained a viscous liquid while the unexposed RF

sample gelled after 9 days at laboratory conditions. The RF gel was observed to have formed a gel 5 days later.



Figure 22: Picture showing differential build-up of silk.

This picture of the second silk experiment shows preferential build-up of silk on one electrode. It is uncertain how long this process took to occur. Throughout the time that the experiment was running, approximately 2 hours, both electrodes appeared to look the same. It was not until after this time that the electrodes were removed from the dish and examined. The gel appears on the more positive electrode appears to be thicker than the gel on the other electrode. The gel like film on the electrode is clear which explains why it was not apparent when the experiment was running in the petri dish, until the receiver was removed from the dish and examined.

Analysis

Coil Experimental Analysis

Comparing the simulated values of the coils individually reveals mixed results. FastHenry simulations of the coils reveals that the predicted values of the inductance of the designed coils were within 10% of what could be measured with an RLC meter for both receiver and transmitter. Comparing the other values measured with the RLC meter shows a greater degree of variability. FastHenry appeared to predict values of less than an Ohm for ESR of both coils, whereas the RLC meter reported values of $2\ \Omega$ and $5\ \Omega$ for the receiver and transmitter respectively. A similar discrepancy is apparent when measuring the quality factor of the inductors individually. The accuracy of the RLC meter is in question since the values obtained from these measurements were so different from the expected simulated values. This could be due to the added resistance of the leads required to measure the coils though the lead length was kept as short as possible to minimize this effect. The leads would affect the resistance of the coils and therefore affect both the ESR and the quality factor of the inductors, but it is unknown to what extent.

Comparing the transmission characteristics of the coils required comparing the simulated coupling coefficients of the coils with the measured parameters of the system. This required manipulating the measured parameters to find the associated coupling coefficient. There is the possibility of measurement error in the parameters measured in the experimental circuit. There is a difference in expected output power from the class E power amplifier. Measuring the input voltage reveals that the function generator used to supply the driving waveforms for the amplifier was not able to supply the 7.5V as this

required a higher current than the generator could give. Despite this class E operation was achieved with the waveforms supplied. Since obtaining a specific output power was not the goal of this circuit this discrepancy does not necessarily affect the desired results of the experiment. The goal of the experiment was to be able to compare the transmission characteristics of the coils with respect to simulated characteristics. For the case of where the coils are moved apart from one another along the same axis, figures 17-19, there appears to be an area where the coils are near each other that disagrees with the simulated results. As the distance between the coils increases the coupling coefficient appears to vary in a manner similar to the simulation in FastHenry. In the log-log plot of these measurements, figure 18, there is clearly an area towards the end of the range that disagrees with the simulated results. This could be due to the presence of noise in the room from external sources that could be affecting the voltages induced in the secondary coil, since the experiment was not performed in a faraday cage this noise could have been present. The log-log plot of the transmission over the range from 0 to 19cm would indicate that the relationship between distance and the coupling between coils has some degree of similarity upon visual inspection and recognizing the variability in the data for the reasons discussed previously; experimental set up and noise within the room. The curve of the simulated results would also indicate that the relationship between the coupling coefficient and distance is not linear as the trend changes over the range of measured data. This is also evident when comparing figure 17 with figure 19, both of these graphs show differences in the curve fitted to the data, showing that parts of the graph may depend differently on distance. Since parts of the graph would seem to have

different relationships with distance this would suggest that the relationship between the coupling coefficient and distance between the coils is not linear.

The graph comparing the variation in coupling when the coils are rotated with respect to each other shows a much greater difference between the simulation and the experimental result. With the test set up used proper alignment between the coils for the increasing separation measurements were more easily maintained than in the rotation experiment. This variation between the simulation parameters and the experimental parameters could account for the differences in the measurements obtained for these experiments.

Silk Experimental Analysis

The first silk experiment examined the differences in the effect that an electromagnetic field would have on an aqueous silk solution. It had been observed in previous research that electrostatic fields appeared to cause silk solutions to gel; though the exact mechanisms of this phenomenon are not fully understood. This experiment used an externally applied electromagnetic field. After approximately an hour and half of exposure to the electromagnetic field there was no apparent difference between the exposed silk solution and the control solution. Both dishes of solution were stored in the lab to observe if there was any perceptible difference in the gelling time between dishes when left in laboratory conditions. This revealed that the exposed petri dish remained liquid after 9 days while the exposed petri dish exhibited the same gelling around 5 days later. This difference in gelling time could indicate an effect of the RF field on the silk solution, but the experiment was not repeated due to time constraints. Since the experiment was not repeated it is uncertain if this result is reliable.

The second experiment modified the receiver used to examine the transmission characteristics to include a diode and a resistor to produce a half-wave rectified output signal generating a polar electric field that was then applied to the silk solution via two electrodes. Minimal separation was maintained between the two electrodes in solution to maximize the applied electric field. While the experiment was running there did not appear to be any gel formation on the electrodes. The electrodes were adjusted at one point during the experiment to try to decrease the electrode spacing, but they were not removed from the solution. It was not until the electrodes were removed from the dish and inspected that it was observed that a clear gel like material had deposited on the more positive electrode. The length that it took this phenomenon to occur is unknown since the electrodes were not periodically inspected throughout the experiment since there was no visible change in the solution.

Discussion

This work demonstrates the derivation of coils designed for transmission in biomedical applications using an iterative method. In order to use the method proposed to design the coils a method of simulating the coil parameters with a particular geometry was required. From this need, VBA code was developed to run simulations of the coil geometries automatically. This work also shows the design of the class E power amplifier, which required knowing the values of the coil parameters. These designed circuits were then implemented on a PCB. The implemented circuits show similar responses when compared to the simulated equivalent in one case where transmission between the coils as a function of distance was explored. In the other transmission experiment a better laboratory set up is required to more accurately complete the test that examines the

effect of rotating one coil with respect to the other. A better setup would allow a more reliable comparison with the simulated effect that this variation has on the coupling between the coils, by more accurately recreating the configurations that were simulated in FastHenry. This work does show a comparison in transmission characteristics between simulated and experimental measurements and successfully demonstrates the transmission of power from transmitter to receiver.

Coil Experimental Discussion

The table below describes the experimental parameters and the possible effect that these parameters have on the transmission between the two coils.

Table 7: Coil parameters and effects on transmission between coils

Input Parameter	Predicted Output Effect	Predicted Relationship with Output
Maximum output voltage peak-peak	Received peak to peak voltage	Higher transmitted voltages would increase the received power
Frequency of operation	Penetration of signal through tissue	Lower transmission frequencies would increase the penetration depth of the signal through tissue
Angle between coils	Received peak to peak voltage	Coil alignment away from parallel decreases received power
Coil geometry	Coupling between coils	Shapes that approach a circle could increase the coupling between the coils
Distance between coils	Received peak to peak voltage	Increasing the distance between coils decreases the received power

If the relationship between the two coils is modeled as a non ideal transformer this yields that the received power is dependent on the amplitude of the voltage across the primary inductor squared. Increasing the amplitude of the peak to peak voltage across the primary inductor would then increase the power in the secondary coil. The frequency of

operation indirectly effects the transmission of the coils by effecting the transmission when the coils are in a medium like tissue as there is a well documented relationship between frequency and penetration depth in tissue where lower frequencies are attenuated less than higher frequencies; for systems that require greater distances between coils lower frequencies are more favorable. Varying the angle between coils changes the degree to which the coils are parallel with each other. This orientation affects the degree that the electromagnetic field incident on the receiver coil is perpendicular; the component of the flux perpendicular to the receiver coil turn surface contributes to the received signal. Simulations in this work showed that the parallel orientation optimized coupling whereas coils that were perpendicular minimized coupling, but this relationship was not clearly demonstrated experimentally. As the surface of the receiver enclosed by the turns of the coil forms a surface that captures the incident magnetic flux increasing this area would increase the incident flux increasing the coupling between the two coils. Increasing the area of the coil requires changing its geometry based on the limitations of the system; for example the receiver coil is limited to one cm in diameter, the maximum area for this geometry would be to construct a circular spiral coil that had a maximum diameter of 1 cm. If the two coils are held parallel to one another there are two ways the coils can move and remain parallel. If both coils lie in the xy plane then the receiver coil can move in the z axis direction or the x axis direction away from the transmitter coil; movement in the y axis direction would be symmetrical to movement in the x axis direction. Movement along this z axis direction was explored in this work. It was found that when compared to simulations of increased separation between the coils in the z direction when the coils are concentric show possibly a similar nonlinear relationship.

Increasing the distance between the coils decreases the amount of coupling between the coils and decreases the amount of power transferred to the receiver.

Silk Experimental Discussion

The table below describes the experimental parameters and possible effects that these have on the output of the system for the silk gel experiments. These possible relationships concern the experiment where the half wave rectified output of the receiver was applied to the silk solution.

Table 8: Experimental parameters and predicted output relationship for silk experiments

Input Parameter	Predicted Output Effect	Predicted Relationship with Output
Maximum received voltage	Final volume of silk gel, rate of gel formation	Higher applied voltages could increase the rate of gel formation
Duty cycle of applied signal	Final volume of silk gel, rate of gel formation	Increasing the duty cycle of the signal would increase the rate of gel formation
Separation between electrodes	Final volume of silk gel, rate of gel formation	For the same voltage decreasing the separation between the electrodes increases the rate of gel formation
Polarity of electrodes	Final volume of silk gel, rate of gel formation	A polar field is required to form a silk gel
Frequency of applied signal	Final volume of silk gel, rate of gel formation	The dependency of gel formation and frequency of applied signal is unknown
Time of exposure	Rate of gel formation	The rate of gel formation should decrease with longer exposure
Ion content of the silk solution	Rate of gel formation	Calcium ion and or potassium content has shown to encourage silk gel formation
pH of the silk solution	Rate of gel formation	Decreasing pH of the solution has been shown to encourage silk gel formation
Silk concentration	Rate of gel formation	Increasing silk protein concentration should increase the rate of silk gel formation

Increasing the amplitude of the voltage of the signal applied to the silk increases the average value of the applied signal, increasing the value of the applied electric field for the same separation between electrodes. The exact mechanism of silk gel formation is unknown, but if as suggested by Lo *et. al.* the mechanism is related to the alignment of charge dipoles within the electric field then increasing the applied voltage will exert a greater force on these dipoles accelerating the alignment of these dipoles with the field and thus increasing the rate of gel formation within the silk solution. Increasing the duty cycle of the pulses applied to the silk solution would have a similar effect as increasing the amplitude of the signal applied to the gel as increasing the duty cycle of the signal increases its average value. If the formation of silk is dependent on the average electric field generated by the signal applied to the silk solution then increasing the average component of this signal would also increase the rate of gel formation. Since the strength of the applied electric field by this reasoning would have an effect on the rate of gel formation decreasing the distance between the electrodes would increase the magnitude of the electric field between the electrodes; an electric field is dependent on the applied voltage and inversely dependent on the separation between the two electrodes. Decreasing the separation between the electrodes would then increase the rate of gel formation by increasing the strength of the applied field for the same voltage. The polarity of the applied field also appears to play a large role in the formation of a silk gel, as demonstrated by Lo *et. al.* when a silk gel forms with one polarity and the polarity of the applied field is switched the generated structure appears to go back into solution. This would imply that a polar field over a non-polar field is necessary to generate a silk gel. In the experiment demonstrated in this work a single frequency of operation was used, this

was because the circuit itself was tuned for operation within a specific frequency range. The results of the receiver applied signal to the silk solutions suggests that it is possible to generate a silk gel with the received signal from the transmitter at this frequency, but this does not yield any information on the dependence of frequency on the formation of a silk gel. Understanding the dependence of the formation of silk gels with frequency would help to optimize the frequency of operation of the system to more effectively form a silk gel. With the dipole alignment model of silk gel formation lower frequencies would allow greater amounts of time for dipoles to randomize during the ‘off’ cycles of the half wave rectified signal possibly decreasing the rate of gel formation. Understanding how the rate of gel formation changes over time is another element that could aid in understanding the mechanism of how a silk gel is formed. As the experiment progresses and a silk gel forms on the electrode this forms a semi solid layer around the electrode which could act like a resistor with different resistive properties of the silk solution itself. Since the silk gel is a more rigid organized structure than the solution itself it may act more like a resistor preventing charges from moving within through the gel. This would mean that through the experiment the charges on the silk protein could be less mobile and the rate of gel formation would then decrease. In previous research ion concentration, pH and silk concentration have been shown to have effects that encourage the formation of silk gels. The relationship between ion concentration and silk gel formation seems to be that increased calcium ion concentration is related to an accelerated rate of gel formation. Similar relationships are observed with lower pH and increased silk fibroin concentration. These parameters of the silk solution could help accelerate the process of silk gel formation when used in combination with the applied signal of the signal, but

understanding the dependence of these factors on the rate of gel formation would be needed to proceed further. In the case of pH, calcium ion concentration and potassium ion concentration, all of the favorable situations involve the presence of more positive charges in solution. It is possible that this factor would repel like charges and possibly encourage favorable conformations between silk proteins increasing the rate constant of the reaction and increasing the rate of silk gel formation.

Understanding the relationships stated above would help improve the system by helping to choose system parameters such as frequency of operation, signal amplitude, duty cycle, separation between the electrodes and silk solution preparation that could have improved results in forming a silk gel.

Future Work

In order to also include a data link in the proposed system modifying the receiver to produce a 5V DC supply voltage to power logic circuits. This would require modifying the receiver to include a bridge diode and voltage regulator along with the necessary capacitor values to produce a 5V DC supply. If the system were to include data transfer the coil geometry used here would need to be evaluated for its ability to transfer data; meaning that the bandwidth of the transmitted and received signals would need to be evaluated since these factors affect the amount of data that can be transmitted.

In designing the system it would have been useful to simulate the function of the circuits prior to constructing them. This was not performed during this research since there was not enough time to learn the necessary simulation software to model the function of the class E power amplifier and the software was unavailable for use.

In taking measurements of the transmission characteristics of the coil measurements that were not along the axis of the coils were more difficult to obtain reliably. It was difficult to maintain the desired orientation when taking measurements for determining the relationship of the angle between the coils and the coupling coefficient. Comparing the simulated with the measured data showed that there was a great difference between these two. A better test set up is needed to hold the coils with the same orientation that was used in the simulations to obtain more relevant results to the simulated data.

In the case of the first silk experiment, more conclusive results on the effect of the presence of an RF field could be obtained if the experiment were run multiple times with the same preparation of silk solution. This would be helpful in determining if the differential gelling times obtained here were repeatable.

If the system is meant to include applications within an implantable system information about the effects of the tissue on the transmission characteristics would be valuable. These effects could be experimentally demonstrated using a similar set up that was used for the experiments performed in this work for analyzing the transmission characteristics between the coils using a tissue phantom to simulate the presence of tissue within the system; for example a certain volume of water with a specific height. This could provide valuable information on the amount of power that would actually be absorbed by tissue.

The mechanism of silk gel formation is largely unknown and the effect of electric fields on the silk solution in the formation of gels could yield valuable information on this process for example. By varying the strength of an electric field by increasing the

applied voltage between two electrodes with a specific separation distance for a certain length of time would show the dependence of silk gel formation on the applied voltage. Similarly if the voltage was held constant but the separation between electrodes was varied this would also affect the applied field strength. Both of these experiments would demonstrate the effect of an applied electric field on the charges present in the silk proteins. If an electric field with greater field strength increases the rate of gel formation then this would indicate that the migration of charges or the orientation of dipoles within the field is an important factor in the formation of a silk gel.

The dependence of the rate of silk gel formation with time is also another important factor. This experiment also requires more knowledge about the electrical properties of the silk gel formed through an electric field to elucidate how its presence affects the mobility of charges. The gel forming on the electrodes of the system forms another element in the system that affects the mobility of charges within the system without affecting the overall applied field. By observing how the rate of gel formation changes with time and the effect of charge mobility and dipole orientation on gel formation can be observed. This would yield information on which of these factors are more important to the mechanism of a silk gel; either charge migration or possible dipole orientation.

The effects of ion content were not observed in these experiments. In future work it would be valuable to add one of the components shown to encourage gel formation to the system to observe the effect of ion concentration in an electric field on the formation of a silk gel. The free charges are likely to be more mobile in solution and migrate in response to the electric field more readily than the silk proteins themselves. The effect

that this might have on silk gel formation would also yield information on how moving charges in solution effects the rate of gel formation.

Appendix

VBA Code for generating FastHenry input files and running simulations

VBA code for individual coils

```
'Cynthia Wisnieff  
'Coil input file generator  
  
Const PI As Double = 3.1415926535898  
Const Resis As Double = 0.000190944
```

```
Sub AutoFHMaker()
```

```
Dim FastHenry2  
Dim RdStart As String  
Dim Location As String  
Dim CoilNumber As Integer  
Dim CCounter As Integer  
Dim CEnd As String  
Dim FileName As String  
Dim FullLocation As String  
Dim CoilID As String  
Dim LResistance As Double
```

```
'Range("C2").Select  
'CoilNumber = ActiveCell.Value  
CoilNumber = 0  
CEnd = Range("A4").Value  
Range("A4").Select
```

```
Do While CEnd <> ""  
    CoilNumber = CoilNumber + 1  
    ActiveCell.Offset(1, 0).Select  
    CEnd = ActiveCell.Value
```

Loop

```
RdStart = "B4"  
Range("C2").Select  
Location = ActiveCell.Value  
Range("E2").Select  
FileName = ActiveCell.Value  
Range("A4").Select  
CoilID = ActiveCell.Value
```

```
' Create FastHenry2 object  
Set FastHenry2 = CreateObject("FastHenry2.Document")
```

```
For CCounter = 1 To CoilNumber  
  ' Try to run FastHenry2  
  ' Remark: the run path must be surrounded by quotas "" to support  
  ' also paths containing spaces (quotas in VisualBasic are escaped by  
  ' doubling the symbol, i.e., "" )  
  FullLocation = Location + FileName + CoilID + ".inp"  
  Call FastHenry2.INPFileMkr(RdStart, FullLocation, LResistance)  
  couldRun = FastHenry2.Run(FullLocation)  
  ' Wait for end of operation, using polling; could also use callback function  
  startTime = Now  
  Do While FastHenry2.IsRunning = True  
    Application.Wait (Now + TimeValue("0:00:01"))  
  Loop  
  ' retrieve capacitance matrix  
  inductance = FastHenry2.GetInductance()  
  Range("M" + CStr((3 + CCounter))).Value = inductance(0, 0, 0)  
  Resistance = FastHenry2.GetResistance()  
  Range("N" + CStr((3 + CCounter))).Value = Resistance(0, 0, 0)  
  Range("P" + CStr((3 + CCounter))).Value = LResistance  
  Range("A4").Select  
  ActiveCell.Offset(CCounter, 0).Select  
  CoilID = ActiveCell.Value  
  ActiveCell.Offset(0, 1).Select  
  RdStart = ActiveCell.Address
```

Next CCounter

```

' Quit FastHenry2
FastHenry2.Quit
' Destroy FastHenry2 object
Set FastHenry2 = Nothing

End Sub

Sub FastHenryINPFileMkr(ParStart As String, SaveFile As String, SeriesR As Double)

' variable declaration
Dim inpFile As String
Dim inpFileNum As Integer
Dim Text As String      ' text to be written
Dim radius As Double
Dim NSides As Integer
Dim STrack As Double    ' Separation between Track
Dim WTrack As Double    ' Width of tracks
Dim NTurns As Integer
Dim Nnodes As Integer   ' Number of Nodes needed
Dim HTrack As Double    ' Track Height
Dim StFreq As Double
Dim EdFreq As Double
Dim Decs As Double
Dim NLayer As Integer
Dim SLayer As Double

Dim DegInc As Double    ' degrees each point will be incremented
Dim RadDec As Double    ' increments distance along each radii
Dim x(100000) As Double, y(100000) As Double, z(100000) As Double ' Arrays for X,
Y and Z coordinates of Nodes
Dim InitRadDec As Double ' decrement radii initially to account for utrn inwards
Dim Counter As Integer   ' Counter for loops
Dim Degree As Double
Dim CurrRad As Double
Dim TurnCount As Integer
Dim Node As Integer
Dim InnerRad As Double
Dim LCount As Integer
Dim ViaDown As Double
Dim Length As Double
Dim Area As Double

LCount = 0
InnerRad = 0

```

```

TurnCount = 0

CurrRad = 0
Degree = 0
Counter = 1

' where file will be stored
inpFile = SaveFile
' Sets up header for file
Text = "***Coil Design File***"
inpFileNum = FreeFile
Open inpFile For Output As inpFileNum
Print #inpFileNum, Text
Text = "*The following line specifies the units for the rest of the file"
Print #inpFileNum, Text
Text = ".Units MM"
Print #inpFileNum, Text
Print #inpFileNum, ""
Text = "*The following sets the default z coordinate to 0 and the conductivity"
Print #inpFileNum, Text
Text = "*to that of copper "
Print #inpFileNum, Text
Text = ".Default z=0 sigma=5.8e4"
Print #inpFileNum, Text
Print #inpFileNum, ""
Print #inpFileNum, ""

' Finds the location of the nodes for a particular geometry input from the spreadsheet
Range(ParStart).Select
radius = ActiveCell.Value
ActiveCell.Offset(0, 1).Select
NSides = ActiveCell.Value
ActiveCell.Offset(0, 1).Select
STrack = ActiveCell.Value
ActiveCell.Offset(0, 1).Select
NTurns = ActiveCell.Value
ActiveCell.Offset(0, 1).Select
WTrack = ActiveCell.Value
ActiveCell.Offset(0, 1).Select
HTrack = ActiveCell.Value
ActiveCell.Offset(0, 1).Select
NLayer = ActiveCell.Value
ActiveCell.Offset(0, 1).Select
SLayer = ActiveCell.Value
ActiveCell.Offset(0, 1).Select
StFreq = ActiveCell.Value

```

```

ActiveCell.Offset(0, 1).Select
EdFreq = ActiveCell.Value
ActiveCell.Offset(0, 1).Select
Decs = ActiveCell.Value

```

```

Nnodes = (NSides * NTurns + 1) * NLayer
DegInc = (2 * PI) / NSides
RadDec = (1 / Sin((PI - DegInc) / 2)) * (STrack + WTrack)
InitRadDec = (STrack + WTrack) / NSides
ViaDown = SLayer + HTrack
CurrRad = radius
Degree = 0
Node = 1
LCount = 1
Area = WTrack * HTrack

```

```

For LCount = 1 To NLayer

```

```

    For TurnCount = 1 To NTurns

```

```

        For Counter = 1 To NSides

```

```

            If (LCount Mod 2) = 1 Then

```

```

                CurrRad = (radius - ((InitRadDec) * (Counter - 1) + (RadDec * (TurnCount - 1))))

```

```

                x(Node) = CurrRad * Cos(Degree)

```

```

                y(Node) = CurrRad * Sin(Degree)

```

```

                z(Node) = ViaDown * (LCount - 1)

```

```

            ElseIf (LCount Mod 2) = 0 Then

```

```

                CurrRad = InnerRad + ((InitRadDec) * (Counter - 1) + (RadDec * (TurnCount - 1)))

```

```

                x(Node) = CurrRad * Cos(Degree)

```

```

                y(Node) = CurrRad * Sin(Degree)

```

```

                z(Node) = ViaDown * (LCount - 1)

```

```

            End If

```

```

        Degree = Degree + DegInc

```

```

        Node = Node + 1

```

```

    Next Counter

```

```

    Counter = 1

```

```

    Degree = 0

```

```

Next TurnCount

```

```

'last node in layer

```

```

If (LCount Mod 2) = 1 Then

```

```

    InnerRad = radius - (RadDec * NTurns)
    x(Node) = (radius - (RadDec * NTurns)) * Cos(0)
    y(Node) = (radius - (RadDec * NTurns)) * Sin(0)
    z(Node) = ViaDown * (LCount - 1)
Else
    'CurrRad = radius
    x(Node) = radius * Cos(0)
    y(Node) = radius * Sin(0)
    z(Node) = ViaDown * (LCount - 1)
End If
Node = Node + 1
Next LCount

Length = 0

For i = 2 To Nnodes - 1

    Length = Sqr((x(i) - x(i - 1)) * (x(i) - x(i - 1)) + (y(i) - y(i - 1)) * (y(i) - y(i - 1))) +
Length
Next i

Length = ViaDown * (NLayer - 1) + Length
SeriesR = (Resis * Length) / Area

'Print to File
Text = "*Nodes of the Polygon"
Print #inpFileNum, Text

Counter = 0
For Counter = 1 To Nnodes
    Text = "N" & Counter & " x=" & x(Counter) & " y=" & y(Counter) & " z=" &
z(Counter)
    Print #inpFileNum, Text

Next Counter

Print #inpFileNum, ""
Print #inpFileNum, ""
Text = "*Segments Connecting Nodes"
Print #inpFileNum, Text
'segments connecting nodes
Counter = 1
For Counter = 1 To (Nnodes - 1)
    Text = "E" & Counter & " N" & Counter & " N" & (Counter + 1) & " w=" & WTrack
& " h=" & HTrack

```

```

    Print #inpFileNum, Text
Next Counter

Print #inpFileNum, ""
Print #inpFileNum, ""

' Port definition
Text = "*Defines a port of the Network"
Print #inpFileNum, Text
Text = ".external N1 N" & Nnodes
Print #inpFileNum, Text

Print #inpFileNum, ""
Print #inpFileNum, ""

Text = "*Frequency Range of Interest"
Print #inpFileNum, Text
Text = ".freq fmin=" & StFreq & " fmax=" & EdFreq & " ndec =" & Decs
Print #inpFileNum, Text

Print #inpFileNum, ""
Print #inpFileNum, ""

Text = ".end"
Print #inpFileNum, Text

Close #inpFileNum

End Sub

```

VBA code for simulating coil pairs

```

'Cynthia Wisnieff
'Coil input file generator

'Option Explicit
Const PI As Double = 3.1415926535898

Sub AutoFHMaker()
Dim FastHenry2
Dim RdStart As String
Dim Location As String
Dim CoilNumber As Integer
Dim CCounter As Integer
Dim CEnd As String

```

```
Dim FileName As String
Dim FullLocation As String
Dim CoilID As String
```

```
CoilNumber = 0
CEnd = Range("A4").Value
Range("A4").Select
```

```
Do While CEnd <> ""
    CoilNumber = CoilNumber + 1
    ActiveCell.Offset(2, 0).Select
    CEnd = ActiveCell.Value
```

```
Loop
```

```
RdStart = "B4"
Range("C2").Select
Location = ActiveCell.Value
Range("E2").Select
FileName = ActiveCell.Value
```

```
RdStart = "B4"
Range("A4").Select
CoilID = ActiveCell.Value
```

```
' Create FastHenry2 object
Set FastHenry2 = CreateObject("FastHenry2.Document")
```

```
For CCounter = 1 To CoilNumber
    ' Try to run FastHenry2
    ' Remark: the run path must be surrounded by quotas "" to support
    ' also paths containing spaces (quotas in VisualBasic are escaped by
    ' doubling the symbol, i.e., "" )
    FullLocation = Location + FileName + CoilID + ".inp"
    Call FastHenryINPFileMkr(RdStart, FullLocation)
    couldRun = FastHenry2.Run(FullLocation)
    ' Wait for end of operation, using polling; could also use callback function
    startTime = Now
    Do While FastHenry2.IsRunning = True
        Application.Wait (Now + TimeValue("0:00:01"))
    Loop
    ' retrieve capacitance matrix
    inductance = FastHenry2.GetInductance()
    Range("Q" + CStr((2 + 2 * CCounter))).Value = inductance(0, 0, 1)
    Range("R" + CStr((2 + 2 * CCounter))).Value = Abs(inductance(0, 0, 1) /
    (Sqr(inductance(0, 0, 0) * inductance(0, 1, 1))))
```

```

Range("S" + CStr((2 + 2 * CCounter))).Value = inductance(0, 0, 0)
Range("T" + CStr((2 + 2 * CCounter))).Value = inductance(0, 1, 1)

Range("A4").Activate
ActiveCell.Offset(2 * CCounter, 0).Select
CoilID = ActiveCell.Value
ActiveCell.Offset(0, 1).Select
RdStart = ActiveCell.Address

Next CCounter

' Quit FastHenry2
FastHenry2.Quit
' Destroy FastHenry2 object
Set FastHenry2 = Nothing

End Sub

Sub FastHenryINPFileMkr(ParStart As String, SaveFile As String)
' variable declaration
Dim inpFile As String
Dim inpFileNum As Integer
Dim Text As String      ' text to be written
Dim radius As Double
Dim NSides As Integer
Dim STrack As Double    ' Separation between Track
Dim WTrack As Double    ' Width of tracks
Dim NTurns As Integer
Dim Nnodes_1 As Integer ' Number of Nodes needed
Dim Nnodes_2 As Integer
Dim HTrack As Double    ' Track Height
Dim StFreq As Double
Dim EdFreq As Double
Dim Decs As Double
Dim NLayer As Integer
Dim SLayer As Double
Dim Zoffset As Double
Dim Xoffset As Double
Dim Yoffset As Double
Dim Rotation As Double

Dim DegInc As Double    ' degrees each point will be incremented
Dim RadDec As Double    ' increments distance along each radii
Dim x(100000) As Double, y(100000) As Double, z(100000) As Double ' Arrays for X,
Y and Z coordinates of Nodes

```

```
Dim R(100000) As Double, Theta(100000) As Double, Zee(1000000) As Double
```

```
Dim InitRadDec As Double ' decrment radii initially to account for utrn inwards  
Dim Counter As Integer ' Counter for loops  
Dim Degree As Double  
Dim CurrRad As Double  
Dim TurnCount As Integer  
Dim Node As Integer  
Dim InnerRad As Double  
Dim LCount As Integer  
Dim ViaDown As Double  
Dim TotLength As Double  
Dim RadRot As Double
```

```
LCount = 0  
InnerRad = 0  
TurnCount = 0  
Const PI As Double = 3.1415926535898  
CurrRad = 0  
Degree = 0  
Counter = 1
```

```
' where file will be stored  
inpFile = SaveFile  
' Sets up header for file  
Text = "***Coil Design File**"  
inpFileNum = FreeFile(0)  
Open inpFile For Output As inpFileNum  
Print #inpFileNum, Text  
Text = "*The following line specifies the units for the rest of the file"  
Print #inpFileNum, Text  
Text = ".Units MM"  
Print #inpFileNum, Text  
Print #inpFileNum, ""  
Text = "*The following sets the default z coordinate to 0 and the conductivity"  
Print #inpFileNum, Text  
Text = "*to that of copper "  
Print #inpFileNum, Text  
Text = ".Default z=0 sigma=5.8e4"  
Print #inpFileNum, Text  
Print #inpFileNum, ""  
Print #inpFileNum, ""  
  
' Finds the location of the nodes for a particular geometry input from the spreadsheet
```

```

Range(ParStart).Select
radius = ActiveCell.Value
ActiveCell.Offset(0, 1).Select
NSides = ActiveCell.Value
ActiveCell.Offset(0, 1).Select
STrack = ActiveCell.Value
ActiveCell.Offset(0, 1).Select
NTurns = ActiveCell.Value
ActiveCell.Offset(0, 1).Select
WTrack = ActiveCell.Value
ActiveCell.Offset(0, 1).Select
HTrack = ActiveCell.Value
ActiveCell.Offset(0, 1).Select
NLayer = ActiveCell.Value
ActiveCell.Offset(0, 1).Select
SLayer = ActiveCell.Value
ActiveCell.Offset(0, 1).Select
StFreq = ActiveCell.Value
ActiveCell.Offset(0, 1).Select
EdFreq = ActiveCell.Value
ActiveCell.Offset(0, 1).Select
Decs = ActiveCell.Value
ActiveCell.Offset(0, 1).Select
Xoffset = ActiveCell.Value
ActiveCell.Offset(0, 1).Select
Yoffset = ActiveCell.Value
ActiveCell.Offset(0, 1).Select
Zoffset = ActiveCell.Value
ActiveCell.Offset(0, 1).Select
Rotation = ActiveCell.Value

Nnodes_1 = (NSides * NTurns + 1) * NLayer
DegInc = (2 * PI) / NSides
RadDec = (1 / Sin((PI - DegInc) / 2)) * (STrack + WTrack)
InitRadDec = (STrack + WTrack) / NSides
ViaDown = SLayer + HTrack
CurrRad = radius
Degree = 0
Node = 1
LCount = 1

TotLength = (NLayer - 1) * HTrack + (NLayer - 1) * SLayer

```

```

For LCount = 1 To NLayer

  For TurnCount = 1 To NTurns

    For Counter = 1 To NSides
      If (LCount Mod 2) = 1 Then
        CurrRad = (radius - ((InitRadDec) * (Counter - 1) + (RadDec * (TurnCount -
1))))
        x(Node) = CurrRad * Cos(Degree)
        y(Node) = CurrRad * Sin(Degree)
        z(Node) = ViaDown * (LCount - 1) - (TotLength / 2)

      ElseIf (LCount Mod 2) = 0 Then
        CurrRad = InnerRad + ((InitRadDec) * (Counter - 1) + (RadDec * (TurnCount
- 1)))
        x(Node) = CurrRad * Cos(Degree)
        y(Node) = CurrRad * Sin(Degree)
        z(Node) = ViaDown * (LCount - 1) - (TotLength / 2)
      End If

      Degree = Degree + DegInc
      Node = Node + 1
    Next Counter
    Counter = 1
    Degree = 0
  Next TurnCount

  'last node in layer
  If (LCount Mod 2) = 1 Then
    InnerRad = radius - (RadDec * NTurns)
    x(Node) = (radius - (RadDec * NTurns)) * Cos(0)
    y(Node) = (radius - (RadDec * NTurns)) * Sin(0)
    z(Node) = ViaDown * (LCount - 1) - (TotLength / 2)
  Else
    'CurrRad = radius
    x(Node) = radius * Cos(0) + Xoffset
    y(Node) = radius * Sin(0) + Yoffset
    z(Node) = ViaDown * (LCount - 1) - (TotLength / 2)
  End If
  Node = Node + 1
Next LCount

'convert to cylindrical with the center of the coil as the center of the coordinate system
' Also adds rotation uses y axis in cartesian as the 'z' axis in cylindrical
Dim nodecount As Integer

```

RadRot = (Rotation) * (PI / 180)

nodecount = 1

For nodecount = 1 To Nnodes_1

R(nodecount) = Sqr(x(nodecount) ^ 2 + z(nodecount) ^ 2)

Theta(nodecount) = Atn(z(nodecount) / x(nodecount))

Zee(nodecount) = y(nodecount)

If x(nodecount) < 0 Then

Theta(nodecount) = PI + Theta(nodecount)

ElseIf x(nodecount) > 0 And z(nodecount) < 0 Then

Theta(nodecount) = 2 * PI + Theta(nodecount)

End If

Theta(nodecount) = Theta(nodecount) + RadRot

Next nodecount

'Conversion back to cartesian

' adds cartesian offsets

For n = 1 To Nnodes_1

x(n) = R(n) * Cos(Theta(n)) + Xoffset

y(n) = Zee(n) + Yoffset

z(n) = R(n) * Sin(Theta(n)) + Zoffset

Next n

'Print to File

Text = "*Nodes of the Polygon"

Print #inpFileNum, Text

Counter = 0

```

For Counter = 1 To Nnodes_1
    Text = "N1_" & Counter & " x=" & x(Counter) & " y=" & y(Counter) & " z=" &
z(Counter)
    Print #inpFileNum, Text

Next Counter

Print #inpFileNum, ""
Print #inpFileNum, ""
Text = "*Segments Connecting Nodes"
Print #inpFileNum, Text
'segments connecting nodes
Counter = 1
For Counter = 1 To (Nnodes_1 - 1)
    Text = "E1_" & Counter & " N1_" & Counter & " N1_" & (Counter + 1) & " w=" &
WTrack & " h=" & HTrack
    Print #inpFileNum, Text
Next Counter

Print #inpFileNum, ""
Print #inpFileNum, ""

'defines the nodes of the second coil
Range(ParStart).Select
ActiveCell.Offset(1, 0).Select
radius = ActiveCell.Value
ActiveCell.Offset(0, 1).Select
NSides = ActiveCell.Value
ActiveCell.Offset(0, 1).Select
STrack = ActiveCell.Value
ActiveCell.Offset(0, 1).Select
NTurns = ActiveCell.Value
ActiveCell.Offset(0, 1).Select
WTrack = ActiveCell.Value
ActiveCell.Offset(0, 1).Select
HTrack = ActiveCell.Value
ActiveCell.Offset(0, 1).Select
NLayer = ActiveCell.Value
ActiveCell.Offset(0, 1).Select
SLayer = ActiveCell.Value
ActiveCell.Offset(0, 1).Select
StFreq = ActiveCell.Value
ActiveCell.Offset(0, 1).Select
EdFreq = ActiveCell.Value
ActiveCell.Offset(0, 1).Select
Decs = ActiveCell.Value

```

```

ActiveCell.Offset(0, 1).Select
Xoffset = ActiveCell.Value
ActiveCell.Offset(0, 1).Select
Yoffset = ActiveCell.Value
ActiveCell.Offset(0, 1).Select
Zoffset = ActiveCell.Value
ActiveCell.Offset(0, 1).Select
Rotation = ActiveCell.Value

Nnodes_2 = (NSides * NTurns + 1) * NLayer
DegInc = (2 * PI) / NSides
RadDec = (1 / Sin((PI - DegInc) / 2)) * (STrack + WTrack)
InitRadDec = (STrack + WTrack) / NSides
ViaDown = SLayer + HTrack
CurrRad = radius
Degree = 0
Node = 1
LCount = 1

For LCount = 1 To NLayer

    For TurnCount = 1 To NTurns

        For Counter = 1 To NSides
            If (LCount Mod 2) = 1 Then
                CurrRad = (radius - ((InitRadDec) * (Counter - 1) + (RadDec * (TurnCount -
1))))
                x(Node) = CurrRad * Cos(Degree)
                y(Node) = CurrRad * Sin(Degree)
                z(Node) = ViaDown * (LCount - 1)

            ElseIf (LCount Mod 2) = 0 Then
                CurrRad = InnerRad + ((InitRadDec) * (Counter - 1) + (RadDec * (TurnCount
- 1)))
                x(Node) = CurrRad * Cos(Degree)
                y(Node) = CurrRad * Sin(Degree)
                z(Node) = ViaDown * (LCount - 1)
            End If

            Degree = Degree + DegInc
            Node = Node + 1
        Next Counter
        Counter = 1
        Degree = 0
    Next TurnCount

```

```

'last node in layer
If (LCount Mod 2) = 1 Then
    InnerRad = radius - (RadDec * NTurns)
    x(Node) = (radius - (RadDec * NTurns)) * Cos(0)
    y(Node) = (radius - (RadDec * NTurns)) * Sin(0)
    z(Node) = ViaDown * (LCount - 1)
Else
    'CurrRad = radius
    x(Node) = radius * Cos(0)
    y(Node) = radius * Sin(0)
    z(Node) = ViaDown * (LCount - 1)
End If
Node = Node + 1
Next LCount

'convert to cylindrical with the center of the coil as the center of the coordinate system
' Also adds rotation uses y axis in cartesian as the 'z' axis in cylindrical

RadRot = (Rotation) * (PI / 180)

nodecount = 1

For nodecount = 1 To Nnodes_2

    R(nodecount) = Sqr(x(nodecount) ^ 2 + z(nodecount) ^ 2)

    Theta(nodecount) = Atn(z(nodecount) / x(nodecount))

    Zee(nodecount) = y(nodecount)

    If x(nodecount) < 0 Then
        Theta(nodecount) = PI + Theta(nodecount)
    ElseIf x(nodecount) > 0 And z(nodecount) < 0 Then
        Theta(nodecount) = 2 * PI + Theta(nodecount)
    End If

    Theta(nodecount) = Theta(nodecount) + RadRot

Next nodecount

```

```
'Conversion back to cartesian
' adds cartesian offsets
```

```
For n = 1 To Nnodes_2
```

```
x(n) = R(n) * Cos(Theta(n)) + Xoffset
y(n) = Zee(n) + Yoffset
z(n) = R(n) * Sin(Theta(n)) + Zoffset
```

```
Next n
```

```
'Print to File
Text = "*Nodes of the Polygon"
Print #inpFileNum, Text
```

```
Counter = 0
For Counter = 1 To Nnodes_2
    Text = "N2_" & Counter & " x=" & x(Counter) & " y=" & y(Counter) & " z=" &
z(Counter)
    Print #inpFileNum, Text
```

```
Next Counter
```

```
Print #inpFileNum, ""
Print #inpFileNum, ""
Text = "*Segments Connecting Nodes"
Print #inpFileNum, Text
'segments connecting nodes
Counter = 1
For Counter = 1 To (Nnodes_2 - 1)
    Text = "E2_" & Counter & " N2_" & Counter & " N2_" & (Counter + 1) & " w=" &
WTrack & " h=" & HTrack
    Print #inpFileNum, Text
Next Counter
```

```
Print #inpFileNum, ""
Print #inpFileNum, ""
```

```
' Port definition
Text = "*Defines a port of the Network"
Print #inpFileNum, Text
```

```

Text = ".external N1_1 N1_" & Nnodes_1
Print #inpFileNum, Text
Text = ".external N2_1 N2_" & Nnodes_2
Print #inpFileNum, Text

Print #inpFileNum, ""
Print #inpFileNum, ""

Text = "*Frequency Range of Interest"
Print #inpFileNum, Text
Text = ".freq fmin=" & StFreq & " fmax=" & EdFreq & " ndec =" & Decs
Print #inpFileNum, Text

Print #inpFileNum, ""
Print #inpFileNum, ""

Text = ".end"
Print #inpFileNum, Text

Close
'#inpFileNum

End Sub

```

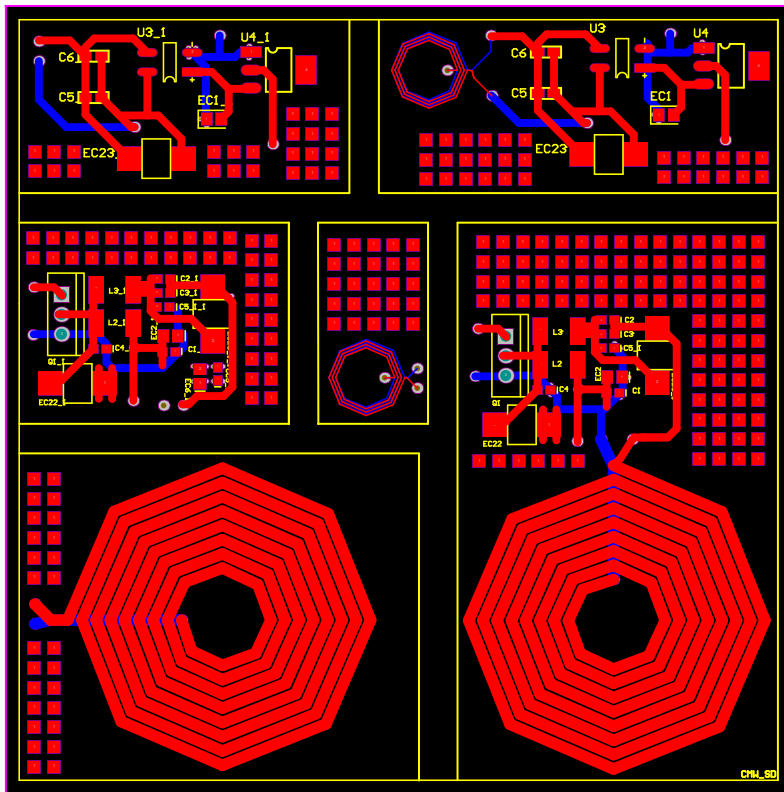


Figure 23: Diagram of PCB used for the final coil designs.

Planar Spiral Coil Pair Maker																			
1	distance are in mm	Coil design location C:\myStuff\	File NameID	Designrotasim															
2	Coil ID	Maximum radius mm	Number of sides N	Width Between Tracks mm	Number of Turns N	Track Width mm	Track Height mm	Number of Layers N	Spacing Between Layers mm	Start Frequency Hz	End Frequency Hz	decades	X offset	Y offset	Z offset mm	rotation in degrees	Make File	Coupling coefficient	self inductance LI
3																			Self inductance L2
4	R0	5	8	0.1778	3	0.2	0.034	2	1.575	13660000	13660000	1	0	0	0	0	1.781E-08	0.023422	3.841E-07
5	-	20	8	0.1778	8	1.5	0.034	1	1.575	13660000	13660000	1	0	0	20	0	1.781E-08	0.023436	3.841E-07
6	-	5	8	0.1778	3	0.2	0.034	2	1.575	13660000	13660000	1	0	0	0	1	1.781E-08	0.023436	3.841E-07
7	-	20	8	0.1778	8	1.5	0.034	1	1.575	13660000	13660000	1	0	0	20	0	1.782E-08	0.023441	3.841E-07
8	R2	5	8	0.1778	3	0.2	0.034	2	1.575	13660000	13660000	1	0	0	0	2	1.782E-08	0.023441	3.841E-07
9	-	20	8	0.1778	8	1.5	0.034	1	1.575	13660000	13660000	1	0	0	20	0	1.782E-08	0.023441	3.841E-07
10	R3	5	8	0.1778	3	0.2	0.034	2	1.575	13660000	13660000	1	0	0	0	3	1.782E-08	0.023441	3.841E-07
11	-	20	8	0.1778	8	1.5	0.034	1	1.575	13660000	13660000	1	0	0	20	0	1.782E-08	0.023441	3.841E-07
12	R4	5	8	0.1778	3	0.2	0.034	2	1.575	13660000	13660000	1	0	0	0	4	1.781E-08	0.023434	3.841E-07
13	-	20	8	0.1778	8	1.5	0.034	1	1.575	13660000	13660000	1	0	0	20	0	1.781E-08	0.023434	3.841E-07
14	R5	5	8	0.1778	3	0.2	0.034	2	1.575	13660000	13660000	1	0	0	0	5	1.786E-08	0.02342	3.841E-07
15	-	20	8	0.1778	8	1.5	0.034	1	1.575	13660000	13660000	1	0	0	20	0	1.786E-08	0.02342	3.841E-07
16	R6	5	8	0.1778	3	0.2	0.034	2	1.575	13660000	13660000	1	0	0	0	6	1.779E-08	0.0234	3.841E-07
17	-	20	8	0.1778	8	1.5	0.034	1	1.575	13660000	13660000	1	0	0	20	0	1.779E-08	0.0234	3.841E-07
18	R7	5	8	0.1778	3	0.2	0.034	2	1.575	13660000	13660000	1	0	0	0	7	1.777E-08	0.023373	3.84E-07
19	-	20	8	0.1778	8	1.5	0.034	1	1.575	13660000	13660000	1	0	0	20	0	1.777E-08	0.023373	3.84E-07
20	R8	5	8	0.1778	3	0.2	0.034	2	1.575	13660000	13660000	1	0	0	0	8	1.774E-08	0.023339	3.84E-07
21	-	20	8	0.1778	8	1.5	0.034	1	1.575	13660000	13660000	1	0	0	20	0	1.774E-08	0.023339	3.84E-07
22	R9	5	8	0.1778	3	0.2	0.034	2	1.575	13660000	13660000	1	0	0	0	9	1.771E-08	0.023290	3.84E-07
23	-	20	8	0.1778	8	1.5	0.034	1	1.575	13660000	13660000	1	0	0	20	0	1.771E-08	0.023290	3.84E-07
24	R10	5	8	0.1778	3	0.2	0.034	2	1.575	13660000	13660000	1	0	0	0	10	1.767E-08	0.02325	3.84E-07
25	-	20	8	0.1778	8	1.5	0.034	1	1.575	13660000	13660000	1	0	0	20	0	1.767E-08	0.02325	3.84E-07
26	R11	5	8	0.1778	3	0.2	0.034	2	1.575	13660000	13660000	1	0	0	0	11	1.763E-08	0.023195	3.84E-07
27	-	20	8	0.1778	8	1.5	0.034	1	1.575	13660000	13660000	1	0	0	20	0	1.763E-08	0.023195	3.84E-07
28	R12	5	8	0.1778	3	0.2	0.034	2	1.575	13660000	13660000	1	0	0	0	12	1.758E-08	0.023134	3.84E-07
29	-	20	8	0.1778	8	1.5	0.034	1	1.575	13660000	13660000	1	0	0	20	0	1.758E-08	0.023134	3.84E-07
30	R13	5	8	0.1778	3	0.2	0.034	2	1.575	13660000	13660000	1	0	0	0	13	1.753E-08	0.023065	3.84E-07
31	-	20	8	0.1778	8	1.5	0.034	1	1.575	13660000	13660000	1	0	0	20	0	1.753E-08	0.023065	3.84E-07
32	R14	5	8	0.1778	3	0.2	0.034	2	1.575	13660000	13660000	1	0	0	0	14	1.747E-08	0.022999	3.84E-07
33	-	20	8	0.1778	8	1.5	0.034	1	1.575	13660000	13660000	1	0	0	20	0	1.747E-08	0.022999	3.84E-07
34	R15	5	8	0.1778	3	0.2	0.034	2	1.575	13660000	13660000	1	0	0	0	15	1.741E-08	0.022906	3.84E-07
35	-	20	8	0.1778	8	1.5	0.034	1	1.575	13660000	13660000	1	0	0	20	0	1.741E-08	0.022906	3.84E-07
36	R16	5	8	0.1778	3	0.2	0.034	2	1.575	13660000	13660000	1	0	0	0	16	1.734E-08	0.022815	3.84E-07
37	-	20	8	0.1778	8	1.5	0.034	1	1.575	13660000	13660000	1	0	0	20	0	1.734E-08	0.022815	3.84E-07
38	R17	5	8	0.1778	3	0.2	0.034	2	1.575	13660000	13660000	1	0	0	0	17	1.727E-08	0.022718	3.84E-07
39	-	20	8	0.1778	8	1.5	0.034	1	1.575	13660000	13660000	1	0	0	20	0	1.727E-08	0.022718	3.84E-07
40	R18	5	8	0.1778	3	0.2	0.034	2	1.575	13660000	13660000	1	0	0	0	18	1.719E-08	0.022613	3.84E-07
41	-	20	8	0.1778	8	1.5	0.034	1	1.575	13660000	13660000	1	0	0	20	0	1.719E-08	0.022613	3.84E-07
42	R19	5	8	0.1778	3	0.2	0.034	2	1.575	13660000	13660000	1	0	0	0	19	1.717E-08	0.022502	3.839E-07
43	-	20	8	0.1778	8	1.5	0.034	1	1.575	13660000	13660000	1	0	0	20	0	1.717E-08	0.022502	3.839E-07
44	R20	5	8	0.1778	3	0.2	0.034	2	1.575	13660000	13660000	1	0	0	0	20	1.701E-08	0.022363	3.839E-07
45	-	20	8	0.1778	8	1.5	0.034	1	1.575	13660000	13660000	1	0	0	20	0	1.701E-08	0.022363	3.839E-07
46	R21	5	8	0.1778	3	0.2	0.034	2	1.575	13660000	13660000	1	0	0	0	21	1.692E-08	0.022259	3.839E-07
47	-	20	8	0.1778	8	1.5	0.034	1	1.575	13660000	13660000	1	0	0	20	0	1.692E-08	0.022259	3.839E-07
48	R22	5	8	0.1778	3	0.2	0.034	2	1.575	13660000	13660000	1	0	0	0	22	1.682E-08	0.022125	3.839E-07
49	-	20	8	0.1778	8	1.5	0.034	1	1.575	13660000	13660000	1	0	0	20	0	1.682E-08	0.022125	3.839E-07
50	R23	5	8	0.1778	3	0.2	0.034	2	1.575	13660000	13660000	1	0	0	0	23	1.671E-08	0.021969	3.839E-07
51	-	20	8	0.1778	8	1.5	0.034	1	1.575	13660000	13660000	1	0	0	20	0	1.671E-08	0.021969	3.839E-07
52	R24	5	8	0.1778	3	0.2	0.034	2	1.575	13660000	13660000	1	0	0	0	24	1.66E-08	0.021837	3.839E-07
53	-	20	8	0.1778	8	1.5	0.034	1	1.575	13660000	13660000	1	0	0	20	0	1.66E-08	0.021837	3.839E-07
54	R25	5	8	0.1778	3	0.2	0.034	2	1.575	13660000	13660000	1	0	0	0	25	1.648E-08	0.021684	3.838E-07
55	-	20	8	0.1778	8	1.5	0.034	1	1.575	13660000	13660000	1	0	0	20	0	1.648E-08	0.021684	3.838E-07
56	R26	5	8	0.1778	3	0.2	0.034	2	1.575	13660000	13660000	1	0	0	0	26	1.636E-08	0.021525	3.838E-07
57	-	20	8	0.1778	8	1.5	0.034	1	1.575	13660000	13660000	1	0	0	20	0	1.636E-08	0.021525	3.838E-07

Figure 24: Screen view of coil pair simulator.

Microsoft Excel - planarspiralcoilmakerandres

File Edit View Insert Format Tools Data Window Help

135% Arial 10

Planar Spiral Coil maker

Coil design location: C:\myStuff File Name: Ccoils .1778 = 7mils Make File

	A	B	C	D	E	F	G	H	I	J	K	L	M	N	O
		Coil design location:	C:\myStuff	File Name:	Ccoils	.1778 = 7mils									
	Coil ID	Maximum radius mm	Number of sides N	Width Between Tracks mm	Number of Turns N	Track Width mm	Track Height mm	Number of Layers N	Spacing Between Layers mm	Start Frequency Hz	End Frequency Hz	decades	Inductance H	Resistance ohm	Q
4	SPC1	5	8	0.18	3	0.2	0.034036	2	1.575	13560000	13560000	1	3.753E-07	0.4089414	78.19
5	SPC2	20	8	0.18	8	1.5	0.034036	1	1.575	13560000	13560000	1	1.477E-06	0.2101626	598.8
6	SPC3	5	8	0.1778	7	0.1	0.034036	1	1.575	13560000	13560000	1	5.366E-07	0.8593184	53.2
7	SPC4	5	8	0.1778	8	0.1	0.034036	1	1.575	13560000	13560000	1	6.226E-07	0.9447764	56.15
8	SPC5	5	8	0.1778	9	0.1	0.034036	1	1.575	13560000	13560000	1	7.009E-07	1.0209097	58.49
9	SPC6	5	8	0.1778	1	0.1	0.034036	1	1.575	13560000	13560000	1	2.993E-08	0.1507369	16.92
10	SPC7	5	8	0.1778	7	0.1	0.034036	1	1.575	13560000	13560000	1	2.71E-06	0.9288288	248.6
11	SPC8	5	8	0.1778	8	0.1	0.034036	1	1.575	13560000	13560000	1	2.865E-06	0.9753174	250.2
12	SPC9	5	8	0.1778	9	0.1	0.034036	1	1.575	13560000	13560000	1	2.92E-06	1.0005306	248.7
13	SPC10	5	8	0.1778	10	0.1	0.034036	1	1.575	13560000	13560000	1	1.665E-06	0.2320951	611.3
14	SPC11	5	8	0.1778	11	0.1	0.034036	1	1.575	13560000	13560000	1	1.755E-06	0.2418736	618.2
15	SPC12	5	8	0.1778	12	0.3	0.034036	1	0.9652	13560000	13560000	1	1.813E-06	0.2492337	619.9
16	SPC13	5	8	0.1778	13	0.3	0.034036	1	0.9652	13560000	13560000	1	1.844E-06	0.2541778	618.2
17	SPC14	5	8	0.1778	14	0.3	0.034036	2	2	13560000	13560000	1	1.854E-06	0.2567169	615.4
18	SPC15	5	8	0.1778	15	0.3	0.034036	2	2	13560000	13560000	1	1.855E-06	0.2574249	614
19	SPC16	5	8	0.1778	16	0.3	0.1	1	2	13560000	13560000	1	2.183E-08	0.0161511	115.1
20	SPC17	5	8	0.1778	17	0.3	0.1	1	0.25	13560000	13560000	1	2.213E-08	0.016327	115.5
21	SPC18	5	8	0.1778	1	0.3	0.1	1	0.25	13560000	13560000	1	2.243E-08	0.016503	115.8
22	SPC19	5	8	0.1778	1	0.3	0.1	1	0.25	13560000	13560000	1	2.273E-08	0.0166789	116.1
23	SPC20	5	8	0.1778	1	0.3	0.1	1	0.25	13560000	13560000	1	2.303E-08	0.0168548	116.4
24	SPC21	5	8	0.1778	1	0.3	0.1	1	0.25	13560000	13560000	1	2.333E-08	0.0170308	116.7
25	SPC22	5	8	0.1778	1	0.3	0.1	1	0.25	13560000	13560000	1	2.363E-08	0.0172067	117
26	SPC23	5	8	0.1778	1	0.3	0.1	1	0.25	13560000	13560000	1	2.394E-08	0.0173827	117.3
27	SPC24	5	8	0.1778	1	0.3	0.1	1	0.25	13560000	13560000	1	2.424E-08	0.0175586	117.6
28	SPC25	5	8	0.1778	1	0.3	0.1	1	0.25	13560000	13560000	1	2.454E-08	0.0177345	117.9
29	SPC26	5	8	0.1778	1	0.3	0.1	1	0.25	13560000	13560000	1	2.485E-08	0.0179105	118.2
30	SPC27	5	8	0.1778	1	0.3	0.1	1	0.25	13560000	13560000	1	2.515E-08	0.0180864	118.5
31	SPC28	5	8	0.1778	1	0.3	0.1	1	0.25	13560000	13560000	1	2.546E-08	0.0182623	118.8
32	SPC29	5	8	0.1778	1	0.3	0.1	1	0.25	13560000	13560000	1	2.577E-08	0.0184383	119.1
33	SPC30	5	8	0.1778	1	0.3	0.1	1	0.25	13560000	13560000	1	2.607E-08	0.0186142	119.3
34	SPC31	5	8	0.1778	1	0.3	0.1	1	0.25	13560000	13560000	1	2.638E-08	0.0187902	119.6
35	SPC32	5	8	0.1778	1	0.3	0.1	1	0.25	13560000	13560000	1	2.669E-08	0.0189661	119.9
36	SPC33	5.6	8	0.1778	1	0.3	0.1	1	0.25	13560000	13560000	1	2.7E-08	0.019142	120.2
37	SPC34	5.65	8	0.1778	1	0.3	0.1	1	0.25	13560000	13560000	1	2.731E-08	0.019318	120.4
38	SPC35	5.7	8	0.1778	1	0.3	0.1	1	0.25	13560000	13560000	1	2.762E-08	0.0194939	120.7

Draw AutoShapes

Figure 25: Screen view of individual coil simulator.

References

1. Atluri S. A wideband power efficient inductive link for implantable biomedical devices using multiple carrier frequencies. 2006.
2. Chandrakasan AP, Verma N, Daly DC. Ultralow-power electronics for biomedical applications. Annual Reviews of Biomedical Engineering. 2008;10:247-74.
3. Reinhold C, Scholz P, John W, Hilleringmann U. Efficient antenna design of inductive coupled RFID-systems with high power demand. Journal of Communications. 2007;2(6):14-23.

4. Gross S, Weller T. Determining the RF resistance and Q-factor of air-core inductors. *Microwave Optical Technology Letters*. 2001;29:89-93.
5. Hambley AR. *Electronics*. 2nd ed. Prentice-Hall, Inc.; 2000.
6. Nilsson JW, Riedel SA. *Electric circuits*. 7th ed. Pearson Prentice Hall; 2005.
7. Sokal NO. *Class-E RF power amplifiers*. ARRL; 2001.
8. 47 CFR part 15. FCC; 1997.
9. Osepchuk JM, Petersen RC. Safety standards: For exposure to RF electromagnetic fields. 2001 June 2001.
10. IEEE standars for safety levels with respect to human exposure to radio frequency electromagnetic fields, 3kHz to 300 GHz. IEEE -SA Standards Board; 1999.
11. Kim U, Park J, Jin H, Valluzzi R, Kaplan DL. Structure and properties of silk hydrogels. *Biomacromolecules*. 2004;5:786-92.
12. Kim J, Rahmat-Samii Y. Implanted antennas inside a human body: Simulations, designs and characterizations. *IEEE Transactions on Microwave Theory and Techniques*. 2004;52(8):1934-43.
13. Lo TJ, Leisk GG, Kaplan DD. Silk electrogelation: Use of a voltage potential for controlled gelation of silk. In press 2009.
14. Sandquist KA. Design of a wireless power and data link for cranially-implanted neural prosthesis [dissertation]. Kansas State University; 2004.

15. Kendir GA, Liu W, Wang G, Sivaprakasam M, Bashirullah R, Humayun MS, et al. An optimal design methodology for inductive power link with class E amplifier. IEEE Transactions on Circuits and Systems. 2005;52.

16. Lou Z. Implementation of A wireless implant system using a high data rate low power BPSK demodulator [dissertation]. Tufts University; 2007.

-